DOI: 10.1002/chem.200903465

Ir-Catalysed Asymmetric Allylic Substitutions with Cyclometalated (Phosphoramidite)Ir Complexes—Resting States, Catalytically Active (π-Allyl)Ir Complexes and Computational Exploration

Jevgenij A. Raskatov, Stephanie Spiess, Christian Gnamm, Kerstin Brödner, Frank Rominger, and Günter Helmchen*[a]

Abstract: Mechanistic aspects of allylic substitutions with iridium catalysts derived from phosphoramidites by cyclometalation were investigated. The determination of resting states by ^{31}P NMR spectroscopy led to the conclusion that the cyclometalation process is reversible. A novel, one-pot procedure for the preparation of (π-allyl)Ir complexes was developed, and these complexes were characterised by X-ray crystal structure analyses and spectral data. They are fully active catalysts of the allylic substitution reaction. DFT calculations on the allyl complexes, transition states of the allylic substitution and product olefin complexes gave further mechanistic insight.

Keywords: allylic compounds · allylic substitution · asymmetric catalysis · iridium · reaction mechanisms

Introduction

The Ir-catalysed allylic substitution has been developed into a reliable tool of organic synthesis over the last few years. The reaction allows preparation of branched, chiral allylic derivatives **2** from readily available monosubstituted allylic substrates **1** with high selectivity (Scheme 1). A broad range of C-, N- and O-nucleophiles can be employed.[1] After probing a variety of Ir complexes the presently best catalysts are generated by base-induced C–H activation from [{Ir(cod)Cl}$_2$] (cod = cycloocta-1,5-diene)[2,3] or [{Ir(dbcot)Cl}$_2$] (dbcot = dibenzocyclooctatetraene)[4] and a chiral phosphoramidite. Several experimental protocols have been developed for the reaction. The salt-free version has proven particularly reliable;[5] this method was originally worked out by Tsuji and co-workers for Rh-catalysed allylic substitutions.[6] It involves production of the nucleophile from its conjugate acid by reaction with carbonate or alkoxide generated in the substitution step. Because of a low content of base and usually homogeneous reaction mixtures in allylic alkylations, the method is also well suited for mechanistic investigations.

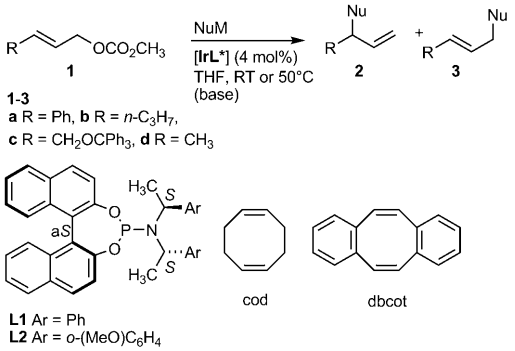

Scheme 1. Ir-catalysed allylic substitution.

We present here a full account of a mechanistic investigation, which addresses several aspects of the Ir-catalysed allylic substitution: 1) Determination of the resting state of the alkylation reaction, which previously was not clearly established. 2) Isolation of a catalytically active (allyl)Ir complex that was elusive at the outset of our investigation. 3) Quantum chemical calculations on experimentally established intermediates of the catalytic cycle.[7]

One result of this study is a remarkably simple and broadly applicable method for preparation of (π-allyl)Ir complexes. Their characterisation by X-ray crystal structure analysis and use as catalysts has furnished considerable in-

[a] Dr. J. A. Raskatov, S. Spiess, Dr. C. Gnamm, K. Brödner, Dr. F. Rominger, Prof. Dr. G. Helmchen
Organisch-Chemisches Institut
Ruprecht-Karls-Universität Heidelberg
Im Neuenheimer Feld 270, 69120 Heidelberg (Germany)
Fax: (+49) 6221-544205
E-mail: g.helmchen@oci.uni-heidelberg.de

Supporting information for this article is available on the WWW under http://dx.doi.org/10.1002/chem.200903465.

sight into the catalytic cycle. We have reported some of the results in a communication.[8] In the meantime we have extended our studies considerably. As ligand, we have mainly employed the particularly effective phosphoramidite **L2** that was introduced by Alexakis et al.[9] Parallel work was carried out by Hartwig et al., who have been using the ligand **L1**.[10,11] They also succeeded in preparing and characterising (π-allyl)Ir complexes, using a preparative procedure, which is different from ours.

A summary of our current view on the mechanism of the Ir-catalysed allylic substitution is given in Scheme 2. Complexes **K1** are formed by simply combining $[\{Ir(cod)Cl\}_2]$ and a phosphoramidite. These complexes are catalytically

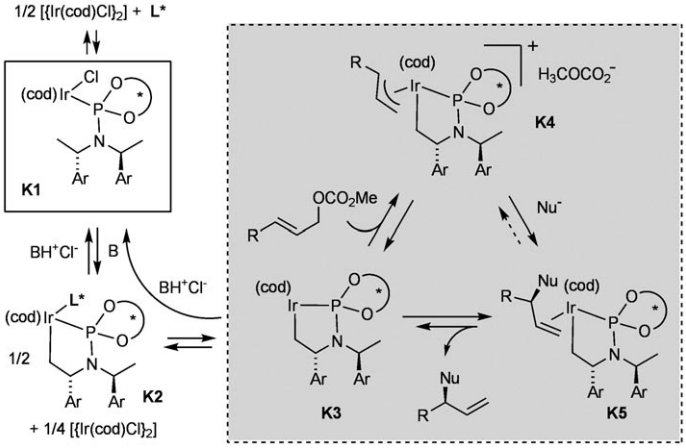

Scheme 2. Catalysis cycle for an allylic substitution reaction using a catalyst prepared in situ from **K1** by treatment with an amine base B; the complex **K1** constitutes the resting state.

inactive, as they do not react with an allylic substrate. Start of a substitution reaction requires the presence of a base, which effects the formation of the cyclometalated complexes **K2** (18 valence electrons (VE)).[3] If the nucleophile is sufficiently basic, as is true, for example, for benzylamine and propylamine, an additional base is not required. Among non-nucleophilic bases TBD (1,5,7-triaza-bicyclo[4.4.0]dec-5-ene) is preferred in our laboratory, because it allows the activation to be carried out in a few minutes. Complex **K2** is not a directly catalytically active species because it is coordinatively saturated; furthermore the reaction rate of an allylic substitution is optimal with a ratio **L***/Ir = 1:1, an excess of **L*** leads to lowering of the reaction rate. As the ligand **L*** of **K2** can be easily replaced by other ligands, the most likely active species in the catalytic cycle is the 16 VE intermediate **K3**.

Results and Discussion

Resting states and (π-allyl)Ir complexes

Resting state of the allylic substitution upon use of an in situ catalyst: Some time ago we have shown[4] that treatment of in situ generated **K2** with weak acids, for example acetic acid, effects the reformation of **K1**. Now we have found that reformation of **K1** also proceeds with allylic substrates and that the catalytically inactive complex **K1** constitutes the resting state of the allylic substitution.

A typical series of experiments was conducted as follows (cf. ^{31}P NMR spectra in Figure 1). Mixing $[\{Ir(cod)Cl\}_2]$ and **L2** (2 equiv) in THF produced the orange complex **K1** (**A** in

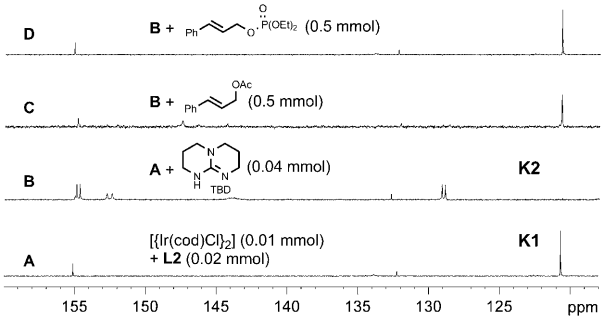

Figure 1. Reversibility of the C–H activation. ^{31}P NMR spectra: **A**) Complex **K1**, generated by reaction of $[\{Ir(cod)Cl\}_2]$ (0.01 mmol) with **L2** (0.02 mmol) in $[D_8]$THF (0.5 mL); **B**) C–H activated species **K2** after 1 h, generated by addition of TBD (0.04 mmol) to solution **A** (**K1**); **C**, **D**) Reformed complex **K1**, measurement 10 min after the addition of cinnamyl acetate or cinnamyl diethyl phosphate (0.5 mmol) to solution **B** (**K2**).

Figure 1). This complex displays a peak at 120.2 ppm and an additional small peak at 131.6 ppm, which corresponds to the hydrido complex **K1H** (see Scheme 3 and the Supporting Information).[12] Addition of TBD effected C–H activation, yielding complex **K2** as a pair of diastereoisomers. The ^{31}P NMR spectrum (**B** in Figure 1) displayed two pairs of doublets that were broadened. Both **K1** and **K2** have been previously described.[4] Addition of an allylic substrate to the solution of **K2** rapidly led to reformation of the complex **K1**. As examples, reactions with cinnamyl acetate (**C**) and cinnamyl diethyl phosphate (**D**) are illustrated by ^{31}P NMR spectra in Figure 1.

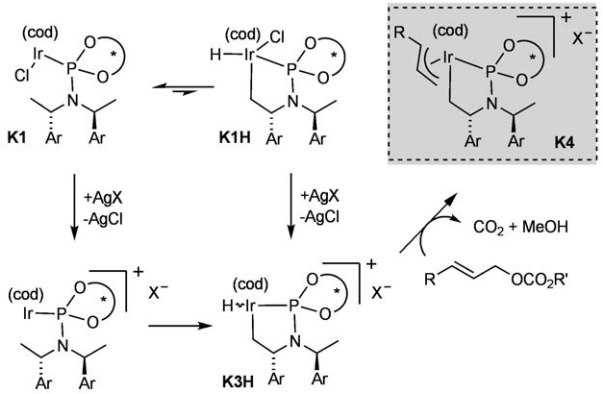

Scheme 3. Formation of (hydrido)Ir complexes **K3H** and allyl complexes **K4**.

A further significant observation concerning the resting state of the allylic substitution was made when ^{31}P NMR spectra were measured during and after completed alkylation and amination reactions (Figure 2). The addition of cinnamyl methyl carbonate and a nucleophile, dimethyl malonate or aniline, to a solution of **K2** in THF led to the reformation of the complex **K1** (**A** and **A′** in Figure 2) in both cases. **K1** remained the major species after completion of the alkylation reaction (**B**). In the case of the completed amination (**B′** in Figure 2), **K1** was accompanied by a second species showing a peak at $\delta_P = 147$ ppm. Hartwig et al.[10] have found a product complex of type **K5** (Scheme 2) for the corresponding reaction upon use of **L1** as ligand ($\delta_P = 148$-150 ppm). Thus, the same type of compound is assumed for the mixture **B′** in Figure 2.[13]

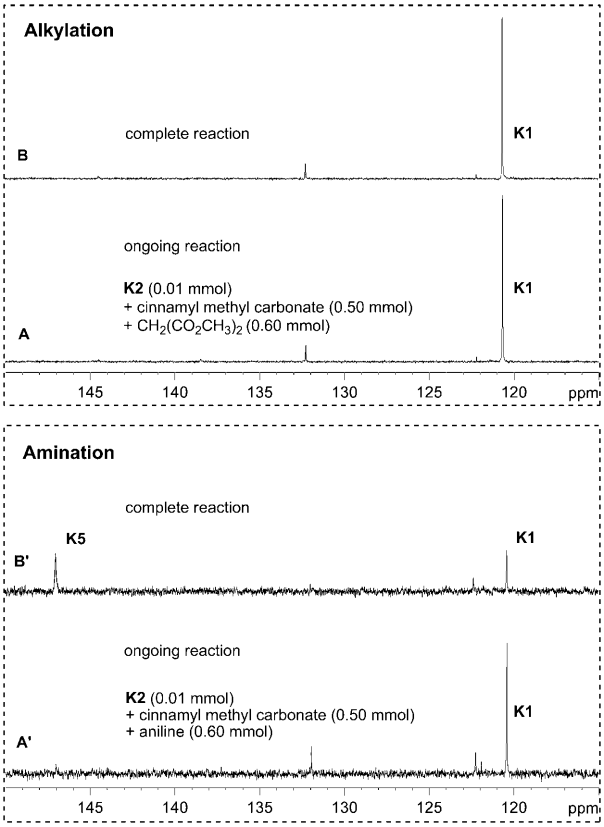

Figure 2. Resting state of the allylic substitution. A solution of **K2** was generated by addition of TBD (0.04 mmol) to a solution of [{Ir(cod)Cl}$_2$] (0.01 mmol) and **L2** (0.02 mmol) in [D$_8$]THF (0.5 mL). ^{31}P NMR spectra: **A**) Reformed complex **K1**, generated by addition of cinnamyl methyl carbonate (0.50 mmol) and $CH_2(CO_2CH_3)_2$ (0.60 mmol) to the solution of **K2**; **B**) Spectrum after 40 min at RT. The reaction was complete; **A′**) Reformed complex **K1**, generated by addition of cinnamyl methyl carbonate (0.50 mmol) and aniline (0.60 mmol) to **K2**; **B′**) Spectrum after >10 h at RT. The reaction was complete.

*Preparation of the (π-allyl)Ir complexes **K4***: The observation that complex **K1** constitutes the resting state of the allylic substitution led us to a very simple method for the preparation of the (π-allyl)Ir complexes of type **K4**. Evidently, a chloride ion and a proton are required for the reformation of **K1**; these must originate from residual [{Ir(cod)Cl}$_2$] and the ammonium salt (BH^+Cl^- in Scheme 2) formed upon catalyst activation by treating **K1** with TBD. We wondered what would be the result of scavenging chloride ions. This was carried out with silver salts; unexpectedly, this directly led to the allyl complexes **K4** (Scheme 4).

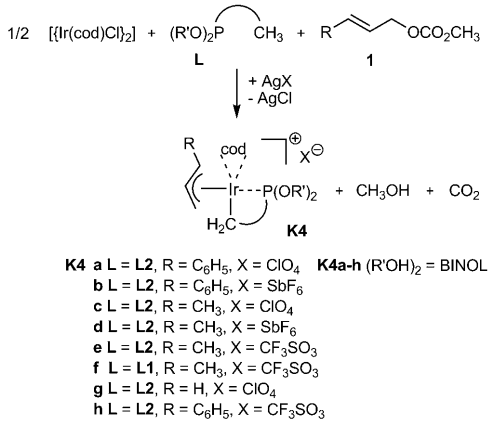

Scheme 4. Synthesis of (π-allyl)Ir complexes from simple components.

Mechanistic aspects of the new method are described for the formation of **K4a**. The preparation was monitored by ^{31}P NMR spectra (Figure 3). First, the complex **K1**, R = Ph, was prepared by mixing [{Ir(cod)Cl}$_2$] and **L2** in THF (**A** in Figure 3).[4] Addition of $AgClO_4$ gave rise to a precipitate of AgCl. The corresponding solution displayed two singlets with an intensity ratio of 3:1 (**B** in Figure 3) in the ^{31}P NMR spectrum. Diastereomers with the constitution **K3H**, X = ClO_4, are assigned to the corresponding compounds (Scheme 3). This assignment is based on the following data. ^1H NMR spectra (not shown) displayed Ir–H resonances at

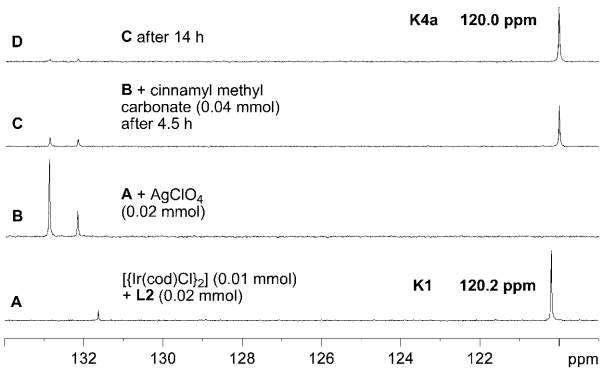

Figure 3. Preparation of **K4a**. ^{31}P NMR spectra: **A**) [{Ir(cod)Cl}$_2$] (0.01 mmol) + (*S*,*S*,*S*)-**L2** (0.02 mmol) (**K1**) in [D$_8$]THF (0.5 mL) after 30 min; **B**) Addition of $AgClO_4$ (0.02 mmol) to solution **A**; **C**) Addition of cinnamyl methyl carbonate (0.04 mmol) to solution **B**, spectrum after 4.5 h at RT; **D**) Spectrum after 14 h at RT.

Table 1. Selected NMR data of the allylic fragment of the (π-allyl)Ir complexes **K4** (numbering of atoms see Figure 5).

	^{1}H NMR [ppm]				^{13}C NMR [ppm]			^{31}P NMR [ppm]
	1_A-H	2_A-H	$3_{A,syn}$-H	$3_{A,anti}$-H	$C1_A$	$C2_A$	$C3_A$	major (minor) isomer
K4a	5.91 (d, J = 12.0 Hz)	4.93–4.99 (m)	2.76–2.90 (m)	2.35 (d, J = 10.8 Hz)	86.51	98.21	41.17	120.0
K4b	5.74 (d, J = 12.4 Hz)	5.05 (ddd, J = 11.6 Hz, 11.6 Hz, 9.7 Hz)	2.77–2.93 (m)	2.09 (d, J = 11.3 Hz)	86.26	98.15	40.63	119.0
K4c	4.85–4.94 (m)	4.22 (ddd, J = 10.7 Hz, 10.7 Hz, 8.5 Hz)	2.84–2.96 (m)	2.20 (d, J = 11.3 Hz)	76.76	107.72	44.71	123.1 (126.6, 4%)
K4d	4.68–4.82 (m)	4.22–4.32 (m)	2.79–2.98 (m)	1.94 (d, J = 11.2 Hz)	76.51	107.70	44.07	122.3 (126.0, 3%)
K4e	4.88–4.95 (m)	4.18–4.24 (m)	2.84–2.94 (m)	2.22–2.41 (m)	76.68	107.72	44.64	123.2
K4f	4.79–4.86 (m)	4.53 (ddd, J = 11.5 Hz, 11.5 Hz, 7.7 Hz)	2.86–2.94 (m)	2.32–2.41 (m)	77.03	107.64	45.20	122.8 (126.2, 2%)
K4h	5.98 (d, J = 12.1 Hz)	4.98 (ddd, J = 11.7 Hz, 11.6 Hz, 7.8 Hz)	2.74–2.91 (m)	2.43 (d, J = 10.9 Hz)	86.52	98.26	41.16	120.2

−24.18 ppm and −21.35 ppm (3:1); the most intense signal of the ESI-FT-ICR-MS possessed the mass of **K3H**$^+$ (m/z calcd and found 900.28). The viability of these (hydrido)Ir complexes was assessed by DFT calculations that are described later. Two likely reaction pathways for their formation are described in Scheme 3, which cannot be distinguished presently.[14]

The solution **B** (Figure 3) was treated with cinnamyl methyl carbonate (**1a**), whereupon the two ^{31}P NMR singlets vanished over a period of 14 h and a singlet at 120.0 ppm appeared (**D** in Figure 3). The corresponding compound was identified by NMR experiments as well as ESI-MS, and a considerable time later also by X-ray crystallography, as the (π-allyl)Ir complex **K4a** (Scheme 4).[15] Methanol formed from the carbonate was detected by ^{1}H NMR spectroscopy. The (π-allyl)Ir complex **K4a** could also be obtained by reaction of **K3H** with cinnamyl acetate or cinnamyl phosphate instead of the carbonate.

The preparation of the (π-allyl)Ir complex **K4a** is described above as a two-step procedure. A one-pot preparation was also feasible and allowed the convenient preparations of the additional complexes **K4b–h** (Scheme 4). The (π-allyl)Ir complexes were found to be stable against oxygen and water, and it was possible to remove trace impurities by conventional column chromatography. Structures of several complexes were determined by X-ray crystal structure analysis (see below).

The formation of **K4a** from **K3H** requires the abstraction of a proton (cf. Scheme 3). Therefore, an additional base might accelerate this step. Indeed, with an excess of NEt_3 as additive complete conversion to **K4a** could be obtained after a reaction time of 15 min rather than 14 h without NEt_3 (see the Supporting Information).

The complexes **K4a** (δ_P = 120.0 ppm), **K4b** (δ_P = 119.0 ppm), **K4e** (δ_P = 123.2 ppm) and **K4h** (δ_P = 120.2 ppm) were obtained isomerically pure (^{31}P NMR spectroscopy). In THF as solvent, the (π-allyl)Ir complex **K4c** displayed a main peak at δ_P = 123.1 ppm and a second peak (4%) at δ_P = 126.6 ppm, as was the case for **K4d** (δ_P = 122.3, 126.0 ppm) and **K4f** (δ_P = 122.8, 126.2 ppm) (Table 1). The second peak (2-4%) originates from an isomer as observed from ^{1}H NMR spectroscopy.

*Allylic substitutions and resting state upon use of (π-allyl)Ir complexes **K4** as catalysts*: Availability of the (π-allyl)Ir complexes allowed their use as catalysts of the allylic substitution. Results of representative substitution reactions obtained with the in situ catalyst and complexes **K4** as catalysts are presented in Table 2. Upon use of complexes **K4** as catalysts under salt free conditions, that is, with $CH_2(CO_2CH_3)_2$ or HNPhth as pronucleophiles, an additional base (TBD) was added in a catalytic amount in order to start the reaction. Under the in situ conditions, TBD was introduced in the activation step. The air stability of the complexes **K4** al-

Table 2. Allylic substitutions corresponding to Scheme 1 using an in situ generated catalyst and complexes **K4** as catalysts.[a]

	R	Pronucleophile [MNu]	Catalyst	Base [mol%]	t [h]	Yield **2+3** [%][b]	**2/3**[c]	ee [%][d]
1	Ph	$CH_2(CO_2CH_3)_2$	in situ	–	2	89	99:1	97
2	Ph	$CH_2(CO_2CH_3)_2$	**K4c**	TBD (8)	0.5	79	98:2	96
3[e]	Ph	$CH_2(CO_2CH_3)_2$	**K4c**	TBD (8)	1.5	60	98:2	96
4	Ph	$NaCH(CO_2CH_3)_2$	in situ	–	0.5	92	99:1	98
5	Ph	$NaCH(CO_2CH_3)_2$	**K4a**	–	0.5	84	99:1	96
6	Ph	$NaCH(CO_2CH_3)_2$	**K4a**	TBD (8)	0.5	86	99:1	98
7	Ph	$NaCH(CO_2CH_3)_2$	**K4b**	–	0.5	85	99:1	97
8	Ph	$NaCH(CO_2CH_3)_2$	**K4h**	–	0.5	84	99:1	98
9	Ph	$NaN(Boc)_2$	in situ	–	0.75	80	97:3	99
10	Ph	$NaN(Boc)_2$	**K4c**	–	3	92	99:1	96
11	Ph	HNPhth	in situ	–	2.5	95	96:4	98
12	Ph	HNPhth	**K4c**	TBD (8)	1	93	96:4	97
13	*n*-Pr	$NaCH(CO_2CH_3)_2$	in situ	–	3	98	89:11	98
14	*n*-Pr	$NaCH(CO_2CH_3)_2$	**K4c**	–	10.5	92	91:9	97
15	*n*-Pr	HNPhth	in situ	–	2.5	82	94:6	96
16	*n*-Pr	HNPhth	**K4c**	TBD (8)	2	88	95:5	96
17	CH_2OCPh_3	$CH_2(CO_2CH_3)_2$	in situ	–	18	90	82:18	99
18	CH_2OCPh_3	$CH_2(CO_2CH_3)_2$	**K4a**	TBD (8)	5	83	79:21	98

[a] Allylic substitution at RT: a) NuH as pronucleophile ("salt-free conditions"): A solution of [{Ir(cod)Cl}$_2$] (2 mol%), **L2** (4 mol%) and TBD (8 mol%) (in situ procedure) or **K4** (4 mol%) in abs. THF (0.5 mL) was prepared; then carbonate **1** (0.5 mmol), a pronucleophile (0.6 mmol) and possibly TBD (8 mol%) were added. b) NaNu as pronucleophile: As in a), however, a freshly prepared solution of NaNu in THF (0.5 mL) was used. [b] Isolated yield. [c] Determined by ^{1}H NMR spectroscopy of crude products. [d] Determined by chiral HPLC (s. Experimental Section). [e] This reaction was carried out without inert atmosphere.

lowed allylic substitutions to be run without an inert atmosphere, which is not possible with the in situ catalysts derived from cod (entry 3). The generally good agreement of the results supports the view that the (π-allyl)Ir complexes are intermediates of the catalytic cycle.

Determination of the resting state of reactions catalysed by a pure allyl complex gave further interesting results (Figure 4). Thus, a reaction mixture prepared from cinnamyl

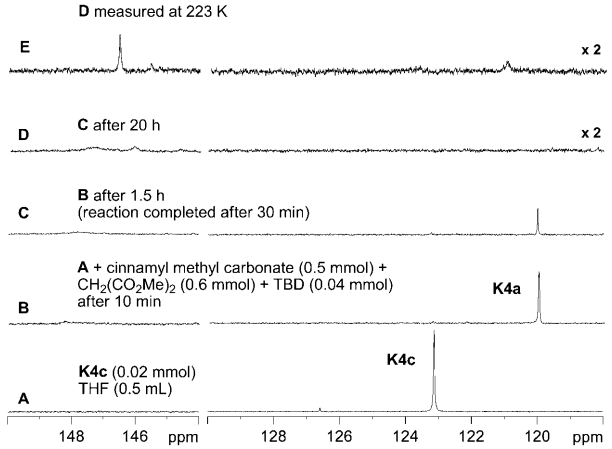

Figure 4. ^{31}P NMR spectra: **A**) **K4c** (0.02 mmol) in [D_8]THF (0.5 mL); **B**) Addition of the carbonate **1a** (0.5 mmol), $CH_2(CO_2Me)_2$ (0.6 mmol) and TBD (0.04 mmol) to solution **A**. Measurement after 10 min at RT; **C**) Measurement after 1.5 h at RT. The reaction was complete after 30 min; **D**) Measurement after 20 h at RT. The spectrum was printed with sensitivity doubled compared to **A**–**C**.

methyl carbonate (**1a**), dimethyl malonate, and catalytic amounts of TBD (8 mol%) and **K4c** (4 mol%) only displayed the ^{31}P NMR peak of the (π-allyl)Ir complex **K4a** after mixing of the reaction partners (Figure 4, **B**). The peak of **K4a** persisted during the reaction and vanished slowly after consumption of the carbonate **1a** (**C**); a very broad peak at $\delta_P = 148$ ppm remained in case of the salt-free reaction (**D**). This peak became sharp upon cooling (**E**). Accordingly, the allyl complex is the resting state of the alkylation, if return to a complex of type **K1** is not possible.

X-ray crystal structures of (π-allyl)Ir complexes: The number of isomeric complexes of the type **K4** amounts to 8 and 16 for the parent π-allyl and monosubstituted π-allyl complexes, respectively (Figure 5, R = H and R ≠ H, respectively). Configurational details could not be determined reliably on the basis of spectroscopic data, and DFT calculations (see below) indicated fairly small energy differences between some of the isomers. Fortunately, our new procedure for preparation of the complexes allowed us to vary the substituent at the allyl moiety and the anion of the complexes quite readily. Crystals of several complexes could be ob-

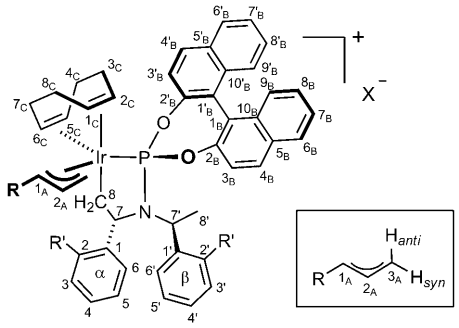

Figure 5. Atom numbering of complexes **K4** and model structures as described in Figure 8.

tained under appropriate crystallisation conditions (Table 3).[16]

As example the structure of the cinnamyl complex **K4b** is displayed in Figure 6. As clearly visible from the CPK model, the 1-phenylallyl moiety sits in a pocket, which surrounds the moiety $C1_A$–$C3_A$ very closely. The pocket is formed by cod, the oxygen of the $(OCH_3)C_6H_4$ group α, one of the O-(1-naphthyl) groups and the aryl group β. The substituent R, here phenyl, protrudes partially; the *ortho*-hydrogen atoms are located at the rim of the pocket. This is likely the cause for the fact that allylic substitutions with *ortho*-substituted cinnamyl derivatives generally proceed with comparatively low degrees of enantioselectivity.[9a,17]

Concerning the steric course of the Ir-catalysed allylic substitution, the following observation is significant. Attack of a nucleophile at $C1_A$ of a π-allyl complex conformationally corresponding to the crystal structure would yield a product with the absolute configuration that has been generally observed experimentally.[1a,18]

Of particular interest are the bond lengths of iridium to the allylic carbon atoms (Table 3). In all examples, the bond

Table 3. Selected bond lengths [Å] and bond angles [°] of the (π-allyl)Ir complexes **K4b**,**d**,**e**,**f**.

	Ir–$C1_A$	Ir–$C2_A$	Ir–$C3_A$	$C1_A$–$C2_A$	$C2_A$–$C3_A$	$C1_A$-$C2_A$-$C3_A$	P-Ir-CH_2	Sum of the bond angles at N	τ(C8′-C7′-N-C7)	τ(Ir-C8-C7-C1)
K4b/1[a]	2.413(8)	2.226 (8)	2.168(8)	1.378(12)	1.406(11)	124.4	74.5	358.4	163.8	−166.4
K4b/2[a]	2.452(9)	2.228(8)	2.173(8)	1.385(13)	1.431(13)	122.5	74.6	358.4	166.5	−163.3
K4d	2.327(12)	2.180(11)	2.201(13)	1.362(16)	1.414(17)	124.8	73.1	354.3	153.3	−169.7
K4e/1[a,b]	2.32(2)	2.172(16)	2.21(2)	1.40(3)	1.44(3)	121.8	73.7	356.1	153.6	−169.6
K4e/2[a,b]	2.377(15)	2.21(2)	2.20(2)	1.39(3)	1.36(3)	123.7	74.3	355.9	161.4	−161.9
K4f	2.355(3)	2.216(3)	2.189(3)	1.404(7)	1.409(6)	121.9	75.5	356.6	145.6	−164.5

[a] The designations "/1" and "/2" refer to independent molecules of the unit cell. [b] The crystal structure analysis was carried out with *ent*-**K4e**.

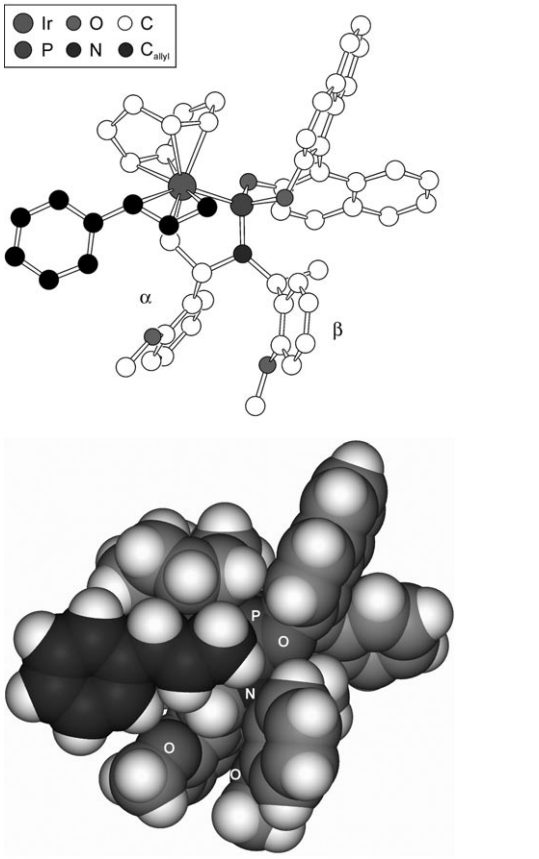

Figure 6. X-ray crystal structure of the cation of complex **K4b** (top: ball and stick model, bottom: CPK model). For a colour figure see the Supporting Information.

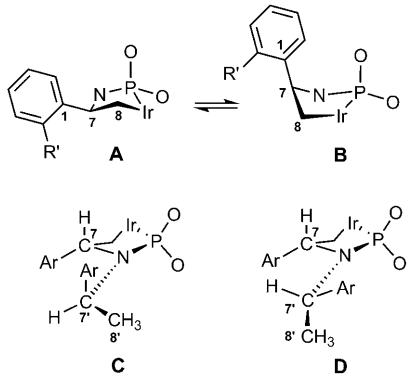

Figure 7. Conformations of the *C,P* chelate ligand of the complexes **K4** and **K4′** (Ar = Ph or *o*-(MeO)C$_6$H$_4$). **K4′** is defined in Figure 9.

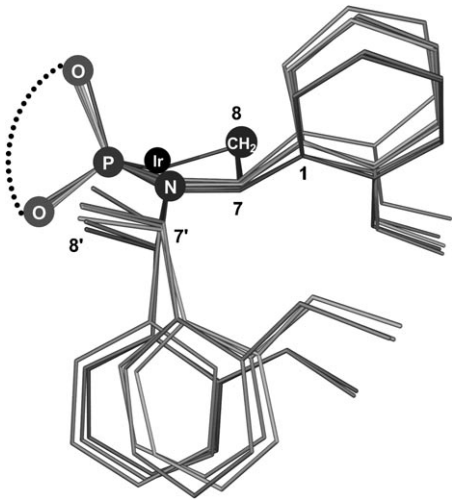

Figure 8. Superposition of the X-ray structures of all (π-allyl)Ir complexes with best fit of the coordination plane [P,Ir,C8]. For a colour figure see the Supporting Information.

to the substituted carbon C1$_A$ is longer than the bond to the unsubstituted C3$_A$, likely due to the strong *trans* influence of P. The difference amounts to 0.15 and 0.26 Å for R = CH$_3$ and Ph, respectively. Thus, the preferred addition of a nucleophile at the higher substituted allylic carbon might be due to preferred breaking of the weaker bond. Bonding within the allylic moiety is almost symmetric as best seen for the crotyl ligand of **K4f**. Even for the cinnamyl ligand, the bond lengths C1$_A$–C2$_A$ and C2$_A$–C3$_A$ differ by maximally 0.04 Å. A similar observation was made previously for a (π-allyl)-(PHOX)Ir complex (PHOX = phoshpino-oxazoline).[15]

The five-membered ring adopts an envelope conformation with an almost planar nitrogen unit and the aryl group α in a pseudoequatorial disposition. The near planarity of the bonds around N is apparent from the value of 356 ± 2° for the sum of the three bond angles. The bond angle P-Ir-C8 of 74 ± 2° is very small because of constraints set by the chelate structure.

The five-membered ring and the 2-arylethyl unit are of further interest since they could exhibit conformational flexibility (cf. Figure 7). A superposition of the corresponding partial structures of all the available X-ray structures containing these units is presented in Figure 8, and geometric data are displayed in Table 3. It is apparent that the conformational data with respect to these two units are similar. Considerable conformational flexibility with respect to the bond C7′–N is apparent from the fact that the torsion angles τ(C8′-C7′-N-C7) vary over a range of 21°, and even for the two structures of **K4e** in the same crystal there is a difference of 8°.

DFT calculations: π-allyl complexes K4′

DFT calculations furnished an interesting insight into the conformational and energetic aspects of the allyl complexes and their reactions. The cyclometalated complexes **K4′** with **L*** = **L3** were primarily used as models; that is, the binaphthyl group was replaced by a biphenyl group and cod by cot (1,3,5,7-cyclooctatetraene) (Figure 9). The latter change was induced by the observation that cod complexes display a twisted, chiral cod moiety requiring the number of models to be doubled in order to account for the helicity of cod. The simplification appears justified because catalysts derived from 2,2′-dihydroxybiphenyl[9,19] or dbcot[4] and cata-

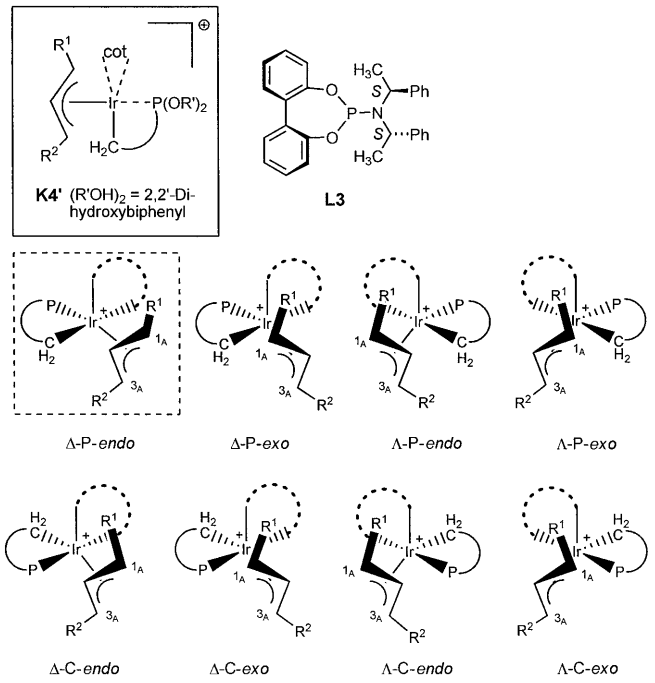

Figure 9. Schematic representations of the configurations of the isomeric (π-allyl)Ir complexes of type **K4** and **K4′**. Formulas in the upper line define the constitution used for DFT calculations; the structure corresponding to the X-ray crystal structure is represented in the box with broken lines. ···=cot; P and C series: one of the allylic carbon atoms is located *trans* to P and the CH_2 group of the *C,P* ligand, respectively; *exo* and *endo*: the $C2_A$–H bond of the allyl ligand is pointing towards cot and away from cot, respectively.

lysts prepared from **L1** or **L2** and cod produce similar results. Ammonia was used as the probe nucleophile. Recently, successful monosubstitution reactions with ammonia as nucleophile have been realised.[20]

The allyl complexes are schematically represented in Figure 9. They are classified into two series, which are designated P- and C-isomers, according to whether one of the allylic termini is located in *trans*-disposition to P or C of the P,C-chelate ligand, respectively.

For our communication,[8] the crystal structure of [Ir(cod)(*C*,*P*-**L1**)PMe_3] (conformer **B**/**D**, cf. Figure 7), as reported by Hartwig et al,[3,21] was used as the starting point for the geometry of the fragment {Ir(*C*,*P*-**L3**)}. The Λ-P-*endo* isomer was found to be the most stable diastereomer in the series of the parent complexes, $R^1=R^2=H$. However, all the subsequently crystallised allylic complexes displayed the Δ-P-*endo* configuration with **A**/**C** as the preferred conformation. To clear this discrepancy, the influence of the conformational degrees of freedom discussed above was investigated computationally. In our preliminary calculations the partial structures **B**/**D** (Figure 7) were used, while in the crystal structures **A**/**C** were found.

*Complexes **K4′**, $R^1=R^2=H$*: First, a conformational curve concerning the phenethyl substituent within the Δ-P-*endo* diastereomer was calculated (Figure 10). It exhibits two minima. The energetically lower one corresponds to the conformer **C**.

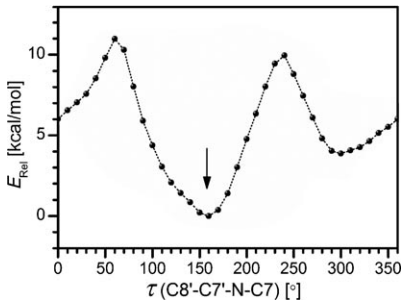

Figure 10. The torsional energy curve of the phenethyl substituent within conformer **A** of the Δ-P-*endo* complex **K4′** ($R^1=R^2=H$); for definition of the torsion angle see Figure 7. Energies refer to gas-phase geometry optimisations; zero-point or THF single-point corrections were not carried out. The arrow denotes the torsional state found in the crystal structure (**C** of Figure 7).

Using conformational orientations **A** and **C** derived from the crystal structures as starting models, calculations on the eight (π-allyl)Ir complexes (**K4′**, $R^1=R^2=H$) were repeated. The results are presented in Table 4 (entry 1). The conformer corresponding to the crystallographically observed one was found to be significantly more stable than the one used in our previous studies (Table 4, entry 6). An exception is the Λ-P-*endo* diastereomer, for which the pseudo-axial orientation **B** was favoured.

The P isomers were found to be more stable than C isomers in the series of the eight (π-allyl)Ir complexes (Table 4). The reason is the lower *trans* influence of P compared to C. Two additional trends are apparent: the *endo* isomers are favoured over *exo* isomers, and there is a clear preference for the Δ- over the Λ-isomers in all cases.

Table 4. DFT energies [kcal mol^{-1}] of allylic complexes **K4′**.[a]

	K4′	Δ-P-*endo*	Δ-P-*exo*	Λ-P-*endo*	Λ-P-*exo*	Δ-C-*endo*	Δ-C-*exo*	Λ-C-*endo*	Λ-C-*exo*
conformers **A** and **C** (cf. Figure 7)									
1	$R^1=R^2=H$	0.0	2.2	3.7	4.7	4.9	5.4	6.2	7.4
2	$R^1=CH_3$, $R^2=H$	0.0	3.2	3.9	4.6	4.1	3.9	7.2	7.0
3	$R^1=H$, $R^2=CH_3$	3.0	4.7	6.6	7.0	6.3	6.7	9.1	9.1
4	$R^1=Ph$, $R^2=H$	0.0	2.5						
5	$R^1=H$, $R^2=Ph$	8.3							
conformers **B** and **D** (cf. Figure 7)									
6	$R^1=R^2=H$	5.6	4.4	3.2	6.6	8.8	8.0	11.2	9.1
7	$R^1=CH_3$, $R^2=H$	4.9	4.6	3.4	7.7	7.4	6.8	9.4	8.1
8	$R^1=H$, $R^2=CH_3$	10.1	7.2	8.1	9.3	12.9	9.8	12.3	10.6

[a] Energies were obtained from gas-phase geometry optimisations with subsequent gas phase zero-point and THF single-point (scrf-cpcm) corrections.

Bonding of the allylic moiety to Ir is non-symmetric (Table 5). In case of the unsubstituted π-allyl ligand, the C–Ir bond *trans* to P or C ($C1_A$–Ir) is longer than the C–Ir bond *trans* to a double bond of the cot ligand ($C3_A$–Ir) for all isomers. The geometric distortion is more pronounced in the C series, as should be expected considering the *trans*-influences of C and P.

*Complexes **K4′**, R^1 or $R^2 = CH_3$*: The 16 model structures were generated from the eight diastereomeric π-allyl complexes by replacing terminal *syn*-hydrogen atoms at $C1_A$ or $C3_A$ of the π-allyl ligand by a methyl substituent (cf. Figure 9). The results of the DFT calculations are presented in Tables 4 and 5. The 1-methylallyl isomers were found to be more stable than the 3-methylallyl isomers by 1.5–3.0 kcal mol^{-1}.

Concerning bond lengths of the crotyl ligand to Ir, in most cases the bond of the methyl-substituted carbon to Ir is longer than that of the unsubstituted terminal carbon (cf. Table 5, entries 9–27).

*Complexes **K4′**, R^1 or $R^2 = Ph$*: Only three of the isomers were investigated (Tables 4 and 5). The Δ-P-*exo* isomer, R^1 = Ph, R^2 = H, was found to be disfavoured by 2.5 kcal mol^{-1} relative to the Δ-P-*endo* isomer; this is consistent with the results obtained for the corresponding allyl complexes **K4′** with $R^1 = R^2 = H$ (2.2 kcal mol^{-1}) and crotyl complexes R^1 = Me, R^2 = H (3.2 kcal mol^{-1}). Interestingly, for the cinnamyl complexes the distance $C1_A$–Ir was calculated to be significantly longer in the Δ-P-*exo* than in Δ-P-*endo* isomer (2.79 vs. 2.63 Å), which seems to result from the repulsive interaction between the phenyl group of the cinnamyl moiety and cot. This is similarly found for the corresponding crotyl complexes, R^1 = Me, albeit to a lesser extent (2.46 vs. 2.55 Å), whereas for the allyl complexes, $R^1 = R^2 = H$, the distance Ir–$C1_A$ is almost identical for the Δ-P-*exo* and the Δ-P-*endo* isomer (2.31 vs. 2.32 Å).

The Δ-P-*endo* isomer with R^1 = H, R^2 = Ph was 8.3 kcal mol^{-1} less stable than the Δ-P-*endo* isomer with the phenyl group at $C1_A$. This is likely due to repulsive interactions between the phenyl group and the $C3_A$ substituent and Ph(β).

DFT calculations: transition states and olefin complexes derived from complexes K4′

Amination transition states were computed for reactions of the thermodynamically favoured isomers Δ-P-*endo*-**K4′** containing the allyl, the crotyl or the cinnamyl ligand. NH_3 was used as the probe nucleophile.

*Reactions at the complex Δ-P-*endo-***K4′**, $R^1 = R^2 = H$: Transition states (TS) and products were located for the addition of NH_3 at $C1_A$, $C2_A$ and $C3_A$ in the case of the unsubstituted allyl complex (Figure 11, R^1 = H). The transition-state energy of the reaction at $C1_A$ was calculated to be 2.8 kcal mol^{-1} lower than that of the reaction at $C3_A$. In ad-

Table 5. Selected bond lengths [Å] and bond angles [°] of the (π-allyl)Ir complexes **K4′**.[a]

	K4′	Configuration	Ir–$C1_A$	Ir–$C2_A$	Ir–$C3_A$	$C1_A$–$C2_A$	$C2_A$–$C3_A$	$C1_A$-$C2_A$-$C3_A$	P-Ir-CH_2
1	$R^1 = R^2 = H$	Δ-P-*endo*	2.31	2.25	2.24	1.41	1.42	121.5	75.7
2	$R^1 = R^2 = H$	Δ-P-*exo*	2.32	2.26	2.24	1.41	1.42	121.4	78.1
3	$R^1 = R^2 = H$	Λ-P-*endo*	2.32	2.25	2.24	1.41	1.42	121.6	73.9
4	$R^1 = R^2 = H$	Λ-P-*exo*	2.35	2.28	2.22	1.40	1.42	121.5	75.9
5	$R^1 = R^2 = H$	Δ-C-*endo*	2.46	2.30	2.20	1.39	1.43	123.2	73.5
6	$R^1 = R^2 = H$	Δ-C-*exo*	2.50	2.32	2.18	1.39	1.44	122.4	75.3
7	$R^1 = R^2 = H$	Λ-C-*endo*	2.42	2.30	2.23	1.40	1.43	122.9	74.1
8	$R^1 = R^2 = H$	Λ-C-*exo*	2.43	2.31	2.22	1.39	1.44	123.2	75.1
9	$R^1 = CH_3$, $R^2 = H$	Δ-P-*endo*	2.46	2.28	2.21	1.40	1.43	123.0	75.6
10	$R^1 = CH_3$, $R^2 = H$	Δ-P-*exo*	2.55	2.32	2.19	1.39	1.44	123.5	77.1
11	$R^1 = CH_3$, $R^2 = H$	Λ-P-*endo*	2.45	2.28	2.20	1.40	1.43	123.2	73.5
12	$R^1 = CH_3$, $R^2 = H$	Λ-P-*exo*	2.59	2.33	2.16	1.39	1.44	123.2	75.6
13	$R^1 = CH_3$, $R^2 = H$	Δ-C-*endo*	2.73	2.37	2.14	1.38	1.45	124.9	74.5
14	$R^1 = CH_3$, $R^2 = H$	Δ-C-*exo*	2.72	2.38	2.15	1.38	1.46	124.6	75.8
15	$R^1 = CH_3$, $R^2 = H$	Λ-C-*endo*	2.68	2.35	2.16	1.38	1.45	124.0	74.4
16	$R^1 = CH_3$, $R^2 = H$	Λ-C-*exo*	2.63	2.36	2.16	1.38	1.45	124.1	74.7
17	$R^1 = H$, $R^2 = CH_3$	Δ-P-*endo*	2.25	2.26	2.36	1.42	1.41	122.0	75.7
18	$R^1 = H$, $R^2 = CH_3$	Δ-P-*exo*	2.28	2.27	2.35	1.41	1.41	122.9	77.0
19	$R^1 = H$, $R^2 = CH_3$	Λ-P-*endo*	2.24	2.28	2.41	1.43	1.40	122.6	73.8
20	$R^1 = H$, $R^2 = CH_3$	Λ-P-*exo*	2.31	2.29	2.31	1.41	1.41	123.6	74.9
21	$R^1 = H$, $R^2 = CH_3$	Δ-C-*endo*	2.36	2.30	2.30	1.41	1.42	123.2	73.6
22	$R^1 = H$, $R^2 = CH_3$	Δ-C-*exo*	2.41	2.31	2.25	1.40	1.43	122.9	74.6
23	$R^1 = H$, $R^2 = CH_3$	Λ-C-*endo*	2.32	2.30	2.35	1.42	1.41	122.5	75.3
24	$R^1 = H$, $R^2 = CH_3$	Λ-C-*exo*	2.40	2.30	2.26	1.40	1.44	124.3	75.4
25	R^1 = Ph, R^2 = H	Δ-P-*endo*	2.63	2.31	2.19	1.40	1.43	124.5	75.5
26	R^1 = Ph, R^2 = H	Δ-P-*exo*	2.79	2.38	2.16	1.39	1.45	124.3	76.7
27	$R^1 = H$, R^2 = Ph	Δ-P-*endo*	2.18	2.35	2.74	1.44	1.39	123.2	76.6

[a] Calculations were carried out using conformational orientations **A**/**C** according to Figure 7.

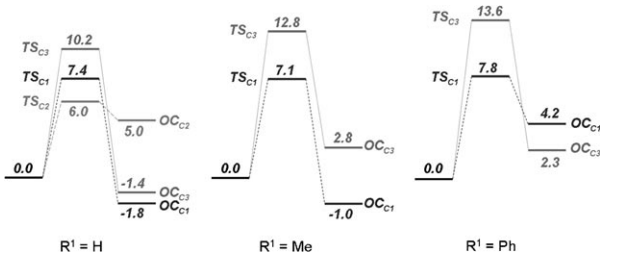

Figure 11. Energy profiles of reactions of complexes Δ-P-*endo*-**K4′**, R^2 = H, with NH_3. Energies were obtained from gas-phase geometry optimisations and subsequent gas-phase zero-point and THF single-point (scrf-cpcm) corrections. TS_{C1} and TS_{C3} = transition states of amination at $C1_A$ and $C3_A$, respectively; OC_{C1} and OC_{C3} = corresponding olefin complexes. For a colour figure see the Supporting Information.

dition, the energy of the resultant olefin complex OC_{C1} of the former reaction is slightly lower.

Reactions at $C2_A$ to give iridacyclobutanes have been observed for Ir complexes by others and by us.[15,22] Interestingly, the activation barrier of the reaction at $C2_A$ was found to be lower than that of the reaction at $C1_A$ (6.0 vs. 7.4 kcal mol^{-1}). However, the resulting iridacyclobutane was found to be energetically unfavorable in comparison with the olefin complexes from the aminations at $C1_A$ and $C3_A$. A rapid, reversible background reaction at $C2_A$, therefore, seems possible. With R^1 = Me and R^1 = Ph it was not possible to locate a transition state or a product of amination at $C2_A$ (see the Supporting Information).

*Reactions at complexes Δ-P-*endo-***K4′**, *R^1 = CH_3 or Ph, R^2 = H*: These calculations also revealed a distinct preference for the addition of NH_3 at $C1_A$, yielding the branched product, over the addition at $C3_A$, yielding the linear product (Figure 11). Of interest is also the relative stability of the product olefin complexes. In the case $R^1 = R^2 = H$ product energies are almost identical, in the case $R^1 = CH_3$, $R^2 = H$, the branched product is preferred over the linear one by 3.8 kcal mol^{-1}; for the cinnamyl derivative, R^1 = Ph, R^2 = H, the Ir complex of the linear product is more stable than that of the branched one by 1.9 kcal mol^{-1}. Thus, there is no correlation between the energies of transition states and the product olefin complexes. In other words, according to these calculations, the regioselectivity of the allylic substitution is not due to product development control.

A description of the geometric change of the system along the reaction path is given by Figure 12 and Table 6. The allylic moiety undergoes a geometric change with only small displacements of the atoms $C2_A$ and $C3_A$ relative to the fragment {Ir(*C*,*P*-**L3**)(cot)}. This movement is best described by a superposition of two rotations. Most pronounced is an out-of-plane rotation about the axis $C2_A$–$C3_A$, as apparent from the torsion angle τ(Ir-$C3_A$-$C2_A$-$C1_A$), which varies by 50–55°. A second component of the allylic motion is clearly seen from the dihedral angle τ(C8-Ir-$C2_A$-$H2_A$) describing an in-plane rotation, which varies over a range of about 15° (Table 6). Viewed in the direction from

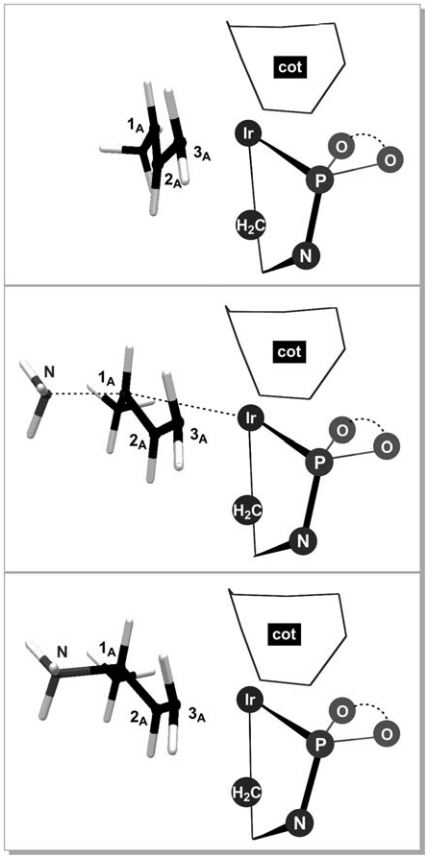

Figure 12. Graphical representation of the reaction of the complex Δ-P-*endo*-**K4′**, $R^1 = CH_3$, R^2 = H, with NH_3 at $C1_A$. For a colour figure see the Supporting Information.

the allylic moiety to iridium, the rotations are clockwise and counter-clockwise for the amination at $C1_A$ and $C3_A$, respectively. A further graphical representation of these movements is given in the Supporting Information.

Possible origin of the minor enantiomer: Possible reaction channels for the formation of the minor enantiomer of the allylic amination with NH_3 were explored for the two π-allyl complexes with Δ-P configuration nearest in energy to the favoured complex Δ-P-*endo*-**K4′**.

The amination at $C3_A$ of the complexes Δ-P-*endo*-**K4′**, R^1 = H, R^2 = Me or Ph, appeared generally unlikely as competing pathways, because of steric crowding in the vicinity of Ph(β) (Figure 6). However, in the case of the crotyl complexes, the relative stabilities of the isomers Δ-P-*endo*-**K4′**, R^1 = H, R^2 = Me and Δ-P-*exo*-**K4′**, R^1 = Me, R^2 = H, are almost identical, 3.0 and 3.2 kcal mol^{-1}, respectively (see Table 4), and the calculated activation barriers are similar, 6.2 and 7.6 kcal mol^{-1} for the reactions of the Δ-P-*exo* isomer at $C1_A$ and the Δ-P-*endo* at $C3_A$, respectively (Figure 13).

After this somewhat unexpected result the cinnamyl derivative Δ-P-*endo*-**K4′**, R^1 = H, R^2 = Ph, was more closely examined, considering that the steric crowding might be re-

Table 6. Selected bond lengths [Å] and torsion angles [°] for the amination of Δ-P-*endo*-**K4′**, R^2 = H.[a] TS_{C1} and TS_{C3} = transition states of amination at $C1_A$ and $C3_A$, respectively; OC_{C1} and OC_{C3} = corresponding olefin complexes.

	R^1		N–C_{react}	Ir–$C1_A$	Ir–$C2_A$	Ir–$C3_A$	C8-Ir-$C2_A$-$C3_A$	C8-Ir-$C2_A$-$C1_A$	C8-Ir-$C2_A$-$H2_A$	Ir-$C3_A$-$C2_A$-$C1_A$	Ir-$C1_A$-$C2_A$-$C3_A$
1	H	allyl complex	∞	2.31	2.25	2.24	123.9	−104.3	10.8	−57.3	56.0
2	H	TS_{C1}	1.93	3.03	2.27	2.15	111.1		−1.6	−96.0	
3	H	OC_{C1}	1.58	3.22	2.20	2.17	106.0		−6.6	−113.8	
4	H	TS_{C3}	2.01	2.18	2.24	2.87		−95.4	18.5		88.0
5	H	OC_{C3}	1.56	2.18	2.18	3.18		−88.5	24.7		112.8
6	Me	allyl complex	∞	2.46	2.28	2.21	120.5	−108.1	8.1	−61.8	56.5
7	Me	TS_{C1}	1.96	3.13	2.27	2.15	110.4		−1.8	−102.8	
8	Me	OC_{C1}	1.59	3.28	2.20	2.16	104.7		−7.2	−117.7	
9	Me	TS_{C3}	1.97	2.24	2.25	2.86		−99.2	14.6		88.8
10	Me	OC_{C3}	1.56	2.22	2.19	3.16		−91.7	20.8		111.0
11	Ph	allyl complex	∞	2.63	2.31	2.19	121.0	−108.8	10.3	−67.6	58.2
12	Ph	TS_{C1}	1.85	3.18	2.25	2.16	109.7		−1.4	−107.5	
13	Ph	OC_{C1}	1.62	3.27	2.20	2.16	105.6		−5.1	−117.2	
14	Ph	TS_{C3}	2.01	2.29	2.24	2.85		−96.6	18.8		90.4
15	Ph	OC_{C3}	1.56	2.25	2.18	3.18		−90.3	23.6		114.2

[a] The model system was generated from the X-ray crystal structure of **K4f** by replacing ligands **L2** by **L3** and cod by cot.

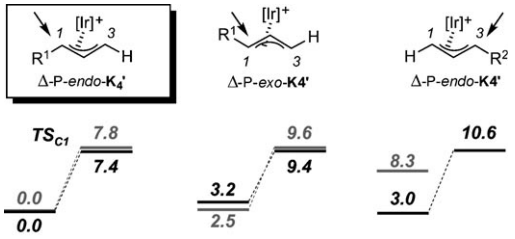

Figure 13. Comparison of the energies along the favoured reaction pathway (left) and two reactions yielding the minor enantiomer (middle and right); R^1 or R^2 = Me (black) and Ph (grey).

lieved by conformational adaptation of the fragment {Ir-(*C*,*P*-**L3**)}. The energies of all conformers according to Figure 7 were calculated and they exceeded 8.3 kcal mol^{-1}. Therefore, the reaction via Δ-P-*endo*-**K4′**, R^1 = H, R^2 = Ph, was not considered viable, and the transition state of its amination was not assessed. Hence, in case of the cinnamyl system the minor enantiomer is likely formed from the Δ-P-*exo* isomer. The calculated activation barrier of 7.1 kcal mol^{-1} is comparable to the 7.8 kcal mol^{-1} calculated for the reaction of the corresponding Δ-P-*endo* isomer at $C1_A$.

We conclude that minor enantiomers are possibly formed by addition of the nucleophiles at $C1_A$ of the Δ-P-*exo* complexes. However, computational assessment of enantioselectivities is not possible at the level of sophistication used here.

DFT calculations: unsimplified allyl complexes K4 and their reactions

With several crystal structures of cod complexes at hand, there was an incentive to carry out calculations on the non-simplified complexes Δ-P-*endo*-**K4**, R^1 = H, Me or Ph, R^2 = H.

*Complexes **K4** with a Δ-P-*endo *configuration*: Representative bond lengths and angles are listed in Table 7. The bond length Ir–$C1_A$ is overestimated computationally by 0.11 Å with R = Me and by 0.21 Å with R = Ph. On the other hand, the difference between the calculated systems **K4** and **K4′** is negligible in both cases. The distance Ir–$C2_A$ is overestimated computationally by 0.09 and 0.08 Å for **K4** and **K4′**, respectively. The bond length Ir–$C3_A$ is well reproduced. Hence B3LYP appears to overestimate the distortion of allylic complexes towards the η^1-coordination mode. Bond angles $C1_A$-$C2_A$-$C3_A$ and P-Ir-C8 are well reproduced by the calculations, whereas for dihedral angles deviations are large. Given that the torsional potentials are generally soft,

Table 7. Comparison of selected bond lengths [Å] and angles [°] from X-ray crystal structures and DFT calculations (Δ-P-*endo* configuration).[a]

	R^1 = Me, R^2 = H			R^1 = Ph, R^2 = H		
	X-ray (**K4d**)	DFT (**K4d**)[b]	DFT (**K4′**)[b]	X-ray (**K4b**)	DFT (**K4b**)[c]	DFT (**K4′**)[c]
Ir–$C1_A$	2.33	2.44	2.46	2.43	2.64	2.63
Ir–$C2_A$	2.18	2.27	2.28	2.23	2.31	2.31
Ir–$C3_A$	2.20	2.21	2.21	2.17	2.19	2.18
$C1_A$–$C2_A$	1.36	1.41	1.40	1.38	1.40	1.40
$C2_A$–$C3_A$	1.42	1.43	1.43	1.42	1.43	1.44
$C1_A$-$C2_A$-$C3_A$	124.8	122.8	123.0	123.5	123.5	124.5
P-Ir-C8	73.1	74.2	75.6	74.6	73.6	75.5
τ(C8′-C7′-N-C7)	153.3	154.3	160.4	165.2	153.4	160.9
τ(Ir-C8-C7-C1)	−169.7	−165.4	−166.1	−164.9	−168.2	−165.8

[a] For the crystal structures, averaged values from the non-equivalent complexes are listed. [b] The starting geometry was derived from the crystal structure of the complex **K4d**. [c] The starting geometry was derived from the crystal structure of the complex **K4b**.

crystal packing effects could exert a considerable influence here.

*Reactions at complexes Δ-P-*endo-***K4***: Results are presented in Figure 14. For all allyl complexes the activation barriers were calculated to be higher by about 1–2 kcal mol^{-1} for the cod than the cot complexes. The complexes of the branched products (OC_{C1}) were found to be less stable than those of the linear products (OC_{C3}). This is a further indication that the regioselectivity of the Ir-catalysed allylic substitution is not controlled by the stability of the product olefin complex.

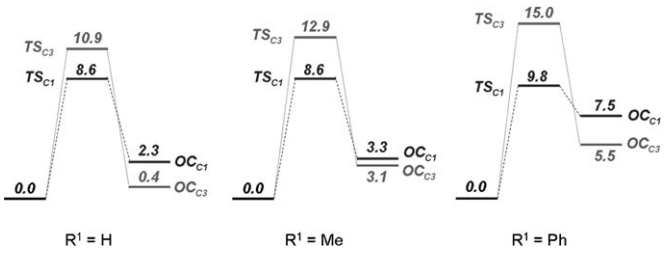

Figure 14. Energy profiles of the reactions of the complexes Δ-P-*endo*-**K4** with NH_3. Energies were obtained from gas-phase geometry optimisations and subsequent gas phase zero-point and THF single-point (scrf-cpcm) corrections. For a colour figure see the Supporting Information.

DFT calculations: hydride complexes [K3′H]$^+$

It was desirable to shed light on the structures of the cationic (hydrido)Ir complexes [**K3H**]$^+$ (cf. Scheme 3). Considering only square pyramidal configurations, there are ten isomers possible (see Figure 15).

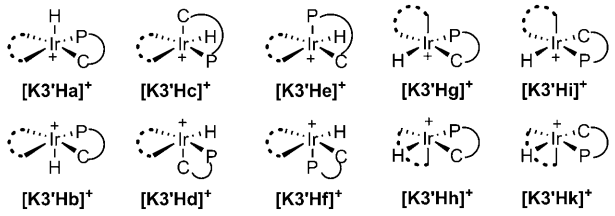

Figure 15. Ten configurationally isomeric (hydrido)Ir complexes [**K3′H**]$^+$. The chelate ligands are as defined in Figure 9.

In addition, there is conformational variability with respect to the iridacycle and the phenethyl group analogous to that described in Figure 7. To assess the viability of these hydride complexes, the topographically distinct model complexes [**K3′H**]$^+$ derived from cot and ligand **L3** were investigated, which should be particularly stable according to consideration of the *trans* influences of the ligands. These isomers were generated by protonation of iridium at the two diastereotopic half-spaces of **K3′**.

Upon consideration of the conformational parameters mentioned above, five conformers of [**K3′Ha**]$^+$ and four conformers of [**K3′Hb**]$^+$ were generated. The two most stable conformers of [**K3′Ha**]$^+$ (both 0.0 kcal mol^{-1}) and the most stable conformer of [**K3′Hb**]$^+$ (0.4 kcal mol^{-1}) are depicted in Figure 16. Note that for once the conformers with a pseudoaxial α phenyl are preferred. The agreement between the calculated relative stabilities of [**K3′Ha**]$^+$ and [**K3′Hb**]$^+$ and the experimentally observed ratio of the cationic hydrides [**K3H**]$^+$ of 3:1 (cf Figure 3) is fortuitous.

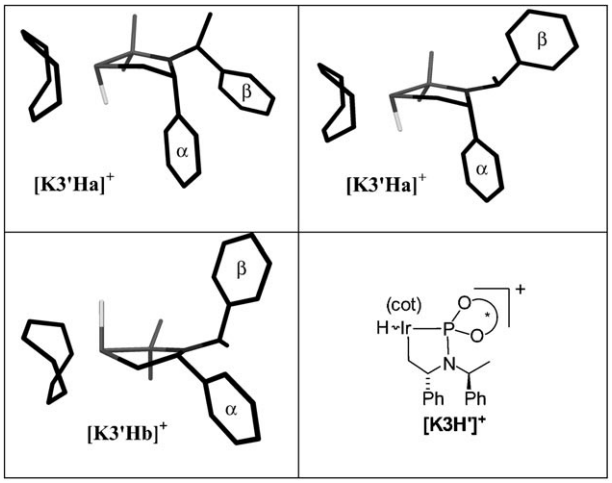

Figure 16. Partial structures of the energetically low conformers of the (hydrido)Ir complexes [**K3′Ha**]$^+$ (both 0.0 kcal mol^{-1}) and [**K3′Hb**]$^+$ (0.4 kcal mol^{-1}) obtained by DFT calculations. For a colour figure see the Supporting Information.

Conclusion

In this article a number of mechanistic aspects of allylic substitutions with iridium catalysts derived from phosphoramidites by C–H activation were investigated. The following main results were obtained:

1) Determination of the resting states by ^{31}P NMR spectroscopy revealed that the C–H activation process is reversible upon use of in situ prepared catalysts.
2) A novel one-pot procedure for the preparation of (π-allyl)Ir complexes from simple starting materials was developed.
3) The new complexes were characterised by X-ray crystal structure analyses and spectral data.
4) The (π-allyl)Ir complexes were found to be fully active catalysts of the allylic substitution reaction and resting states under conditions, which excluded reversion of the C–H activation.
5) Finally, DFT calculations on the allyl complexes, transition states of the allylic substitution and product olefin complexes were carried out on both slightly simplified and unsimplified complexes.

Experimental Section

Computational methods: All computations were performed using the hybrid Becke functional (B3)[23] for electron exchange and the correlation

functional of Lee, Yang and Parr (LYP),[24] as implemented in the GAUSSIAN 03 software package.[25] For iridium, the SDD basis set with the associated effective core potential was employed.[26] All other atoms were modelled at the 6-31G(d) level of theory.[27] Geometry optimisations were performed without any symmetry constraints (C_1 symmetry).

Starting geometries for the transition state search were located by performing restricted geometry optimisations. The distance between the reacting carbon terminus and the nitrogen nucleophile was fixed at 2.0 Å for the nucleophilic attack at $C1_A$ or $C3_A$ and 1.9 Å for reactions at $C2_A$, respectively. The thus obtained geometries were subsequently fully optimised as saddle points of first-order, employing the Berny algorythm.[28] Frequency calculations were undertaken to confirm the nature of the stationary points, yielding zero imaginary frequencies for all allyl and olefin complexes. The amination transition states possessed one imaginary frequency, which represented the vector of the C–N bond formation in all cases. Zero-point energy corrections were carried out for all computed energies. The solvent influence was additionally taken into account by conducting single-point polarised continuum (CPCM-SCRF) calculations,[29] with THF ($\varepsilon = 7.6$) as the solvent.[30]

General: Unless stated otherwise, reactions were carried out under argon using anhydrous conditions. ^{1}H NMR spectra were recorded at RT on the following spectrometers: Bruker AC-300 (300 MHz), Bruker Avance 500 (500 MHz). The spectra were recorded in $CDCl_3$ or [D_8]THF and chemical shifts are reported in δ units relative to TMS or to the residual undeuterated solvent ($CHCl_3$ in $CDCl_3$ at $\delta_H = 7.26$ ppm).[31] The following abbreviations are used to indicate the signal multiplicity: s (singlet), d (doublet), t (triplet), q (quartet), m (multiplet), dd (doublet of doublets), dt (doublet of triplets), ddd (doublet of doublets of doublets), brs (broad signal). ^{13}C NMR spectra were recorded at RT on the following spectrometers: Bruker AC-300 (75.48 MHz), Bruker Avance 500 (125.76 MHz). The spectra were recorded in $CDCl_3$ or [D_8]THF and chemical shifts are reported in δ units relative to the residual undeuterated solvent $CHCl_3$ ($\delta_C = 77.16$ {central line of the triplet})[31] The following abbreviations were used: s (singlet, quarternary C-atom), d (doublet, CH-group), t (triplet, CH_2-group), q (quartet, CH_3-group). The multiplicity stated refers to {^{1}H}-decoupled spectra. ^{31}P NMR spectra were recorded at RT on the following spectrometers: Bruker DRX-250 (101.26 MHz), Bruker AC-300 (121.50 MHz), Bruker Avance 500 (202.46 MHz). The spectra were recorded in $CDCl_3$ or [D_8]THF and chemical shifts are reported in δ units relative to TMS in ^{1}H NMR spectra[32] or phosphoric acid or triphenylphosphine as external standard. The assignments of signals for compounds **K4a–f** were confirmed by H,H-COSY, H,C-COSY, TOCSY, HMBC, NOESY and DEPT spectra. Atom numbers are specified at the formulas. ^{1}H NMR spectra of all new compounds are presented in the Supporting Information. High-resolution mass spectra were recorded on a Bruker ApexQe FT-ICR (ESI+) mass spectrometer. X-ray data were collected on a Bruker APEX diffractometer equipped with a $Mo_{K\alpha}$ radiation source ($\lambda = 0.71073$ Å) and a graphite monochromator. Intensities were corrected for Lorentz and polarisation effects; an empirical absorption correction was applied using SADABS.[33] All structures were solved by direct methods and refined against F^2 using the SHELXTL software package.[34] The corresponding crystallographic data are displayed in Table 8. CCDC-756243 (**K4b**), -756244 (**K4d**), -738902 (**K4e**) and -756245 (**K4f**) contain the supplementary crystallographic data for this paper. These data can be obtained free of charge from The Cambridge Crystallographic Data Centre via www.ccdc.cam.ac.uk/data_request/cif. Flash-column chromatography was carried out with silica gel (0.032–0.062) of Macherey, Nagel and Co. Tetrahydrofuran was dried over benzophenone ketyl, and the water content was determined by Karl Fischer titration. 1,5,7-Triazabicyclo[4.4.0]dec-5-ene (TBD) was stored in a desiccator over KOH. IUPAC names were generated by the ACD/Labs 6.0 programm from Advanced Chemistry Development Inc.

Syntheses, spectroscopic data and determinations of enantiomeric excesses of the following compounds were already reported: **1c**,[35] **2a**, Nu = $CH(CO_2CH_3)_2$,[36] **2a**, Nu = N(Boc)$_2$,[5] **2a**, Nu = NPhth,[5] **2b**, Nu = NPhth,[5] **2c**, Nu = $CH(CO_2CH_3)_2$.[36] In the case of **2b**, Nu = $CH(CO_2CH_3)_2$,[9] a Krapcho reaction was carried out (NaCl (1.2 equiv), H_2O (6 equiv), DMSO, 160 °C, 14 h) and the product was analysed by GC: Hewlett Packard Gas Chromatograph 5890$_A$, column Varian CP-Chirasil-Dex (β-CD), 25 m × 0.25 mm × 0.25 μ, isothermal, 70 °C, 24.7 min, 26.1 min.

Table 8. Data of the crystal structure analysis of the (π-allyl)Ir complexes.

	K4b	**K4d**	**K4e**	**K4f**
formula	$C_{55}H_{54}F_6IrNO_4PSb \cdot {}^1/_2C_6H_6$	$C_{50}H_{52}F_6IrNO_4PSb \cdot 3C_6H_6$	$C_{51}H_{52}F_3IrNO_7PS \cdot 3C_6H_6$	$C_{49}H_{48}F_3IrNO_5PS \cdot 2C_6H_6$
M_r	1290.97	1424.17	1337.49	1199.33
crystal size [mm^3]	0.14 × 0.12 × 0.10	0.30 × 0.17 × 0.05	0.31 × 0.26 × 0.12	0.27 × 0.24 × 0.16
crystal system	monoclinic	orthorhombic	triclinic	monoclinic
space group	$P2_1$	$P2_12_12_1$	$P\bar{1}$	$P2_1$
a [Å]	13.6182(8)	12.184(2)	12.4002(16)	11.6538(15)
b [Å]	20.5836(12)	17.401(3)	15.0182(19)	20.556(3)
c [Å]	18.6485(11)	29.009(5)	17.062(2)	12.4857(16)
α [°]	90	90	89.086(3)	90
β [°]	93.604(1)	90	89.860(3)	116.433(2)
γ [°]	90	90	76.275(3)	90
V [Å^3]	5217.1(5)	6150.7(18)	3086.4(7)	2678.3(6)
Z	4	4	2	2
ρ_{calcd} [g cm^{-3}]	1.64	1.54	1.44	1.49
μ [mm^{-1}]	3.17	2.69	2.29	2.62
max/min tranmission	0.74/0.67	0.88/0.50	0.77/0.54	0.68/0.54
index ranges	$-18 \le h \le 18$	$-15 \le h \le 15$	$-15 \le h \le 15$	$-15 \le h \le 15$
	$-27 \le k \le 27$	$-21 \le k \le 21$	$-18 \le k \le 18$	$-27 \le k \le 27$
	$-24 \le l \le 24$	$-36 \le l \le 36$	$0 \le l \le 21$	$-16 \le l \le 16$
θ range [°]	1.9–28.4	1.4–26.4	1.9–26.4	2.0–28.3
T [K]	200(2)	200(2)	200(2)	200(2)
reflns collected	55479	55907	12548	28505
independent reflns [R_{int}]	25676 [0.0505]	12566 [0.0604]	12552 [0.0000]	13025 [0.0204]
observed reflns [$I > 2\sigma(I)$]	22210	10780	11621	12519
data/restraints/parameters	25676/13/1285	12566/435/767	12552/210/1426	13025/25/675
GOF on F^2	1.09	1.16	1.13	1.03
final R_1/wR_2 indices [$I > 2\sigma(I)$]	0.057/0.113	0.077/0.158	0.046/0.109	0.024/0.056
absolute structure parameter	0.020(4)	0.019(10)	0.091(10)	−0.014(3)
max/min residual [e Å^{-3}]	2.35/−1.80	5.43/−1.32	1.52/−0.72	1.07/−0.41

General procedure for the preparation of (π-allyl)Ir complexes (GP1): In a flame-dried Schlenk tube under an argon atmosphere, complex **K1** was prepared by stirring a solution of [{Ir(cod)Cl}$_2$] (6.7 mg, 10 μmol) and **L***(20 μmol) in dry THF (0.5 mL, <30 μg H_2O mL^{-1} THF, Karl–Fischer titration) at room temperature for the stated time. The allylic carbonate (30 or 40 μmol) and AgX (20 μmol) were added to the orange solution causing the formation of a white precipitate. The mixture was stirred for 20 min and kept at room temperature for the stated time. The white precipitate was removed by centrifugation and/or filtration, and the excess of carbonate was removed with the solvent under reduced pressure or by flash column chromatography (silica gel, dichloromethane, then dichloromethane/isopropanol 97:3–95:5).

General procedure for the allylic substitutions according to Scheme 1 (GP2): Allylic substitution: a) NuH as pronucleophile ("salt-free conditions"): In a dry Schlenk flask under argon, a solution of [{Ir(cod)Cl}$_2$] (2 mol%), **L2** (4 mol%) and TBD (8 mol%) (in situ procedure) or **K4c** (4 mol%) in absolute THF (0.5 mL) was prepared; then carbonate **1** (0.5 mmol), a pronucleophile (0.6 mmol) and possibly TBD (8 mol%) were added and conversion monitored by TLC. b) NaNu as pronucleophile: As in a), however, a solution of NaNu in THF (0.5 mL), which was freshly prepared from NuH (0.6 mmol) and NaH (0.6 mmol), was used.

K4a: According to GP1 [{Ir(cod)Cl}$_2$] (40.3 mg, 60.0 μmol) and (*R*,*R*,a*R*)-**L2** (72.0 mg, 120.0 μmol) were stirred in dry THF (3 mL) at room temperature for 30 min. Cinnamyl methyl carbonate (49.9 mg, 260.0 μmol) and $AgClO_4$ (24.6 mg, 120.0 μmol) were added. After 20 h the formed white precipitate was removed by filtration, and the crude product was subjected to flash column chromatography (silica gel, dichloromethane, then dichloromethane/isopropanol 97:3) to yield **K4a** (115.2 mg, 86%) as a light yellow powder. ^{1}H NMR (500.13 MHz, [D$_8$]THF): $\delta=8.41$ (d, $J=8.6$ Hz, 1H; BINOL), 8.31 (d, $J=8.9$ Hz, 1H; BINOL), 8.12 (d, $J=8.5$ Hz, 1H; BINOL), 8.10 (d, $J=8.5$ Hz, 1H; BINOL), 8.03 (d, $J=8.8$ Hz, 1H; BINOL), 7.93 (d, $J=9.0$ Hz, 1H; BINOL), 7.86–7.88 (m, 2H; 2×Ph$_{Allyl}$), 7.24–7.57 (m, 13H; 4×Ph, 6×BINOL, 3×Ph$_{Allyl}$), 7.08–7.13 (m, 2H; 2×Ph), 6.99 (dd, $J=7.5$, 7.5 Hz, 1H; 4-H), 6.93 (d, $J=8.3$ Hz, 1H; 6-H), 5.91 (dd, $J_{P,H}=12.0$ Hz, $J=12.0$ Hz, 1H; 1$_A$-H), 5.34–5.38 (m, 1H; cod-CH), 4.93–4.99 (m, 1H; 2$_A$-H), 4.67 (dd, $J=11.6$, 4.9 Hz, 1H; 7-H), 4.48–4.57 (m, 1H; 7′-H), 4.11 (s, 3H; OCH_3), 3.95–4.01 (m, 1H; cod-CH), 3.89–3.94 (m, 1H; cod-CH), 3.58 (s, 3H; OCH_3), 2.76–2.90 (m, 4H; cod-CH, 2×cod-CH_2, 3$_{A,syn}$-H), 2.56–2.64 (m, 1H; cod-CH_2), 2.35 (d, $J=10.8$ Hz, 1H; 3$_{A,anti}$-H), 2.19–2.31 (m, 2H; cod-CH_2, 8b-H), 2.10–2.13 (dd, $J=14.7$, 8.2 Hz, 1H; cod-CH_2), 1.76–1.79 (m, 1H; cod-CH_2), 1.55–1.62 (m, 1H; cod-CH_2), 1.41–1.51 (m, 1H; cod-CH_2), 0.90 (dd, $J=12.0$, 12.0 Hz, 1H; 8a-H), 0.48 ppm (d, $J=7.4$ Hz, 3H; 8′-H); ^{13}C-{^{1}H,^{31}P} NMR (125.76 MHz, [D$_8$]THF): $\delta=157.85$, 157.76, 149.83, 148.69 (s; 4×Ph), 135.92 (s; Ph$_{Allyl}$), 133.95, 133.42 (s; 2×Ph), 133.10 (d; BINOL), 133.03, 132.29 (s; 2×Ph), 132.19 (d; BINOL), 131.70 (s; Ph), 130.09, 129.96, 129.96, 129.87, 129.67, 129.60, 129.46, 129.29, 128.77 (d; 3×Ph, 2×BINOL, 2×Ph$_{Allyl}$, s; Ph), 127.95, 127.74, 127.69, 127.69, 126.82, 126.81 (d; 6×BINOL), 124.84 (d; Ph), 123.71 (s; Ph), 123.02, 122.31 (d; 2×BINOL), 122.13 (s; Ph), 121.51, 121.33, 111.28, 111.20 (d; 4×Ph), 102.42 (d; CH-cod), 98.21 (d; C-2$_A$), 92.72, 90.44 (d; 2×CH-cod), 86.51 (d; C-1$_A$), 83.65 (d; CH-cod), 60.44 (d; C-7), 55.82, 55.24 (q; 2×OCH_3), 53.21 (d; C-7′), 41.17 (t C-3$_A$), 35.62, 34.03, 28.41, 26.93 (t; 4×CH_2-cod), 19.24 (q; C-8′), 14.84 ppm (t; C-8); ^{31}P NMR (202.46 MHz, [D$_8$]THF): $\delta=120.01$ ppm; HRMS (ESI+): *m*/*z* calcd for $C_{55}H_{54}IrNO_4P^+$: 1016.3414; found: 1016.3409 $[M]^+$.

K4b: According to GP1 [{Ir(cod)Cl}$_2$] (16.8 mg, 25.0 μmol) and (*R*,*R*,a*R*)-**L2** (30.0 mg, 50.0 μmol) were stirred in dry THF (1.3 mL) at room temperature for 30 min. Cinnamyl methyl carbonate (19.2 mg, 100 μmol) and $AgSbF_6$ (>20 mg (17.2 mg≡50.0 μmol)) were added. After 20 h the formed white precipitate was removed by filtration, and the crude product was subjected to flash column chromatography (silica gel, dichloromethane/isopropanol 97:3) to yield **K4b** (43.6 mg, 70%) as an orange powder. A saturated solution of **K4b** in THF, treated with benzene, deposited crystals suitable for X-ray diffraction. These were isolated by filtration. ^{1}H NMR (500.13 MHz, [D$_8$]THF): $\delta=8.40$ (d, $J=9.0$ Hz, 1H; BINOL), 8.27 (d, $J=9.0$ Hz, 1H; BINOL), 8.12 (d, $J=8.5$ Hz, 1H; BINOL), 8.10 (d, $J=9.0$ Hz, 1H; BINOL), 7.93 (d, $J=9.0$ Hz, 1H; BINOL), 7.81–7.86 (m, 3H; BINOL, 2×Ph$_{Allyl}$), 7.53–7.58 (m, 3H; Ph, BINOL), 7.43–7.49 (m, 4H; Ph, 3×Ph$_{Allyl}$), 7.34–7.40 (m, 4H; 4×BINOL), 7.25–7.33 (m, 2H; 2×Ph), 7.09–7.13 (m, 2H; 2×Ph), 6.98 (dd, $J=7.3$, 7.3 Hz, 1H; Ph), 6.95 (d, $J=7.9$ Hz, 1H; Ph), 5.74 (d, $J=12.4$ Hz, 1H; 1$_A$-H), 5.26–5.31 (m, 1H; cod-CH), 5.05 (ddd, $J=11.6$, 11.6, 9.7 Hz, 1H; 2$_A$-H), 4.73 (dd, $J=11.2$, 4.5 Hz, 1H; 7-H), 4.51–4.57 (m, 1H; 7′-H), 4.12 (s, 3H; OCH_3), 4.04–4.09 (m, 1H; cod-CH), 3.57–3.63 (m, 4H; cod-CH, OCH_3), 2.77–2.93 (m, 3H; 3$_{A,syn}$-H, cod-CH_2), 2.45–2.53 (m, 1H; cod-CH_2), 2.12–2.35 (m, 3H; 8b-H, 2×cod-CH_2), 2.09 (d, $J=11.3$ Hz, 1H; 3$_{A,anti}$-H), 1.79–1.86 (m, 1H; cod-CH_2), 1.57–1.64 (m, 1H; cod-CH_2), 1.44–1.52 (m, 1H; cod-CH_2), 0.97 (dd, $J=12.2$, 12.2 Hz, 1H; 8a-H), 0.49 ppm (d, $J=7.3$ Hz, 3H; 8′-H); ^{13}C{^{1}H,^{31}P} NMR (125.76 MHz, [D$_8$]THF): $\delta=157.90$, 157.77, 149.77, 148.51 (s, 4×Ph), 135.52 (s; Ph$_{Allyl}$), 133.91, 133.49, 133.00, 132.97 (s; 4×Ph), 132.86, 132.29 (d; 2×BINOL), 131.43 (s; Ph), 130.14, 130.11, 129.98 (d; 2×Ph, Ph$_{Allyl}$), 129.87 (s; Ph), 129.57, 129.56, 129.50, 129.47 (d; 2×BINOL, 2×Ph$_{Allyl}$), 128.93 (d; Ph), 128.04, 127.95, 127.75, 127.64, 126.98, 126.92 (d; 6×BINOL), 124.86 (d; Ph), 123.59 (s; Ph), 122.33, 122.32, 122.20 (d; 2×BINOL, s; Ph), 121.54, 121.20, 111.30 (d; 4×Ph), 101.77 (d; CH-cod), 98.15 (d; C-2$_A$), 92.57, 91.22 (d; 2×CH-cod), 86.26 (d; C-1$_A$), 84.25 (d; CH-cod), 55.75, 55.25 (q; 2×OCH_3), 53.29 (d; C-7′), 40.63 (t; C-3$_A$), 35.71, 33.93, 28.36, 27.00 (t; 4×CH_2-cod), 19.16 (q; C-8′), 15.11 ppm (t; C-8); ^{31}P NMR (121.50 MHz, [D$_8$]THF): $\delta=118.96$ ppm; HRMS (ESI+): *m*/*z* calcd for $C_{55}H_{54}IrNO_4P^+$: 1016.3414; found: 1016.3452 $[M]^+$.

K4c: According to GP1 [{Ir(cod)Cl}$_2$] (40.4 mg, 60.0 μmol) and (*S*,*S*,a*S*)-**L2** (71.9 mg, 120.0 μmol) were stirred in dry THF (3 mL) at room temperature for 30 min. Crotyl methyl carbonate (33.1 mg, 250.0 μmol) and $AgClO_4$ (26.2 mg, 130.0 μmol) were added. After 6 h the formed white precipitate was removed by filtration, and the crude product was subjected to flash column chromatography (silica gel, dichloromethane, then dichloromethane/isopropanol 95:5) to yield **K4c** (129.3 mg, 99%) as a light yellow powder containing 4% of an isomeric by-product. All analytical data given refers to a 96:4 mixture of the isomers (ratio determined by ^{31}P NMR spectroscopy). ^{1}H NMR (500.13 MHz, [D$_8$]THF, major isomer): $\delta=8.39$ (d, $J=9.0$ Hz, 1H; BINOL), 8.26 (d, $J=8.5$ Hz, 1H; BINOL), 8.11 (d, $J=7.9$ Hz, 1H; BINOL), 8.08 (d, $J=8.5$ Hz, 1H; BINOL), 7.93 (d, $J=8.5$ Hz, 1H; BINOL), 7.91 (d, $J=8.5$ Hz, 1H; BINOL), 7.49–7.56 (m, 3H; Ph, 2×BINOL), 7.43 (d, $J=7.3$ Hz, 1H; Ph), 7.30–7.39 (m, 4H; 4×BINOL), 7.19–7.27 (m, 2H; 2×Ph), 7.06–7.11 (m, 1H; Ph), 6.99 (d, $J=7.9$ Hz, 1H; Ph), 6.89–6.96 (m, 2H; 2×Ph), 5.17–5.24 (m, 1H; cod-CH), 4.85–4.94 (m, 1H; 1$_A$-H), 4.42–4.52 (m, 2H; 7-H, 7′-H), 4.22 (ddd, $J=10.7$, 10.7, 8.5 Hz, 1H; 2$_A$-H), 3.98–4.06 (m, 1H; cod-CH), 3.88 (s, 3H; OCH_3), 3.54 (s, 3H; OCH_3), 3.32–3.39 (m, 1H; cod-CH), 3.21–3.30 (m, 1H; cod-CH_2), 3.11–3.18 (m, 1H; cod-CH), 2.84–2.96 (m, 2H; 3$_{A,syn}$-H, cod-CH_2), 2.33–2.42 (m, 1H; cod-CH_2), 2.24–2.32 (m, 1H; cod-CH_2), 2.20 (d, $J=11.3$ Hz, 1H; 3$_{A,anti}$-H), 2.03–2.10 (m, 2H; cod-CH_2, 8b-H), 1.85 (dd, $J=8.8$, 6.0 Hz, 3H; CH_3), 1.59–1.67 (m, 1H; cod-CH_2), 1.40–1.56 (m, 2H; 2×cod-CH_2), 0.81 (dd, $J=12.1$, 12.1 Hz, 1H; 8a-H), 0.43 ppm (d, $J=7.3$ Hz, 3H; 8′-H); ^{13}C{^{1}H,^{31}P} NMR (125.76 MHz, [D$_8$]THF, major isomer): $\delta=157.89$, 157.80, 149.87, 148.73, 133.95, 133.43 (s; 6×Ph), 132.96 (d; BINOL), 132.88, 132.88 (s; 2×Ph), 132.09 (d; BINOL), 131.92, 130.08 (s; 2×Ph), 129.89, 129.82 (d; 2×Ph), 129.54, 129.44 (d; 2×BINOL), 128.63 (d; Ph), 127.88, 127.68, 127.68, 127.65, 126.74, 126.73 (d; 6×BINOL), 124.97 (d; Ph), 123.70 (s; Ph), 122.93, 122.43 (d; 2×BINOL), 122.18 (s; Ph), 121.36, 121.15, 111.35, 111.12 (d; 4×Ph), 107.72 (d; C-2$_A$), 102.93, 91.71, 88.22, 83.09 (d; 4×CH-cod), 76.76 (d; C-1$_A$), 60.57 (d; C-7 or C-7′), 55.63, 55.17 (q; 2×OCH_3), 53.11 (d; C-7 or C-7′), 44.71 (t; C-3$_A$), 37.27, 35.64, 28.48, 26.19 (t; 4×CH_2-cod), 19.22 (q; C-8′), 15.31 (q; CH_3), 12.13 ppm (t; C-8); ^{31}P NMR (202.46 MHz, [D$_8$]THF, major isomer): $\delta=123.14$ ppm; HRMS (ESI+): *m*/*z* calcd for $C_{50}H_{52}IrNO_4P^+$: 954.3258; found: 954.3248 $[M]^+$.

K4d: According to GP1 [{Ir(cod)Cl}$_2$] (33.6 mg, 50.0 μmol) and (*R*,*R*,a*R*)-**L2** (60.0 mg, 100.0 μmol) were stirred in dry THF (2.5 mL) at room temperature for 30 min. Crotyl methyl carbonate (26.0 mg, 200.0 μmol) and an excess of $AgSbF_6$ (40–50 mg (34.4 mg≡100.0 μmol)) were added. After 20 h the formed white precipitate was removed by filtration, and the crude product was subjected to flash column chromatography (silica gel, dichloromethane, then dichloromethane/isopropanol 97:3) to yield **K4d** (86.4 mg, 73%) as a yellow powder containing 3% of

an isomeric by-product. All analytical data given refers to a 97:3 mixture of the isomers (ratio determined by ^{31}P NMR spectroscopy). A saturated solution of **K4d** in THF, treated with benzene, deposited crystals suitable for X-ray diffraction. These were isolated by filtration. ^1H NMR (300.13 MHz, [D$_8$]THF, major isomer): $\delta = 8.39$ (d, $J = 8.9$ Hz, 1H; BINOL), 8.23 (d, $J = 8.7$ Hz, 1H; BINOL), 8.12 (d, $J = 8.4$ Hz, 1H; BINOL), 8.09 (d, $J = 8.4$ Hz, 1H; BINOL), 7.92 (d, $J = 8.7$ Hz, 1H; BINOL), 7.75 (d, $J = 8.9$ Hz, 1H; BINOL), 7.50–7.59 (m, 3H; Ph, 2× BINOL), 7.24–7.43 (m, 7H; 3×Ph, 4×BINOL), 7.09 (dd, $J = 7.6$, 7.6 Hz, 1H; Ph), 7.01 (d, $J = 8.1$ Hz, 1H; Ph), 6.91–6.96 (m, 2H; 2×Ph), 5.11–5.19 (m, 1H; cod-CH), 4.68–4.82 (m, 1H; 1$_A$-H), 4.41–4.55 (m, 2H; 7-H, 7′-H), 4.22–4.32 (m, 1H; 2$_A$-H), 4.02–4.13 (m, 1H; cod-CH), 3.90 (s, 3H; OCH$_3$), 3.58 (s, 3H; OCH$_3$), 3.19–3.35 (m, 2H; cod-CH, cod-CH$_2$), 3.07–3.15 (m, 1H; cod-CH), 2.79–2.98 (m, 2H; 3$_{A,syn}$-H, cod-CH$_2$), 2.25–2.38 (m, 2H; 2×cod-CH$_2$), 2.08–2.20 (m, 2H; 8b-H, cod-CH$_2$), 1.94 (d, $J =$ 11.2 Hz, 1H; 3$_{A,anti}$-H), 1.88 (dd, $J = 8.9$, 6.1 Hz, 3H; CH$_3$), 1.40–1.77 (m, 3H, 3×cod-CH$_2$), 0.86 (dd, $J = 11.5$, 11.5 Hz, 1H; 8a-H), 0.44 ppm (d, $J =$ 7.5 Hz, 3H; 8′-H); $^{13}C\{^1H,^{31}P\}$ NMR (125.76 MHz, [D$_8$]THF, major isomer): $\delta = 157.90$, 157.86, 149.81, 148.55, 133.91, 133.51, 132.92, 132.92 (s, 8×Ph), 132.60, 132.20 (d, 2×BINOL), 131.64, 130.05 (s, 2×Ph), 129.96, 129.82, 129.48, 129.48, 128.78 (d, 3×Ph, 2×BINOL), 127.98, 127.92, 127.76, 127.59, 126.91, 126.84 (d, 6×BINOL), 124.91 (d; Ph), 123.58 (s; Ph), 122.38, 122.34, 122.27 (d, 2×BINOL, s; Ph), 121.35, 120.97, 111.38, 111.21 (d; 4×Ph), 107.70 (d; C-2$_A$), 102.33, 91.50, 88.88, 83.51 (d; 4×CH-cod), 76.51 (d; C-1$_A$), 60.62 (d; C-7 or C-7′), 55.59, 55.16 (q; 2×OCH$_3$), 53.13 (d; C-7 or C-7′), 44.07 (t; C-3$_A$), 37.19, 35.73, 28.42, 26.20 (t; 4×CH$_2$-cod), 19.12 (q; C-8′), 15.18 (q; CH$_3$), 12.29 ppm (t; C-8); ^{31}P NMR (202.46 MHz, [D$_8$]THF, major isomer): $\delta = 122.33$ ppm; HRMS (ESI+): m/z calcd for $C_{50}H_{52}IrNO_4P^+$: 954.3258; found: 954.3279 $[M]^+$.

K4e: According to GP1 [{Ir(cod)Cl}$_2$] (33.6 mg, 50.0 μmol) and (*S*,*S*,a*S*)-**L2** (60.0 mg, 100.0 μmol) were stirred in dry THF (2.5 mL) at room temperature for 30 min. Crotyl methyl carbonate (26.0 mg, 200.0 μmol) and AgOTf (26.0 mg, 100.0 μmol) were added. After 20 h the formed white precipitate was removed by filtration, and the crude product was subjected to flash column chromatography (silica gel, dichloromethane/isopropanol 97:3) to yield **K4e** (98.2 mg, 88%) as a light yellow powder. A saturated solution of **K4e** in THF, treated with benzene, deposited crystals suitable for X-ray diffraction. These were isolated by filtration. ^1H NMR (500.13 MHz, [D$_8$]THF): $\delta = 8.38$ (d, $J = 9.0$ Hz, 1H; BINOL), 8.25 (d, $J = 9.0$ Hz, 1H; BINOL), 8.11 (d, $J = 8.5$ Hz, 1H; BINOL), 8.08 (d, $J =$ 8.5 Hz, 1H; BINOL), 7.89–7.93 (m, 2H; 2×BINOL), 7.49–7.55 (m, 3H; Ph, 2×BINOL), 7.43 (d, $J = 7.3$ Hz, 1H; Ph), 7.31–7.38 (m, 4H; 4× BINOL), 7.21–7.27 (m, 2H; 2×Ph), 7.08 (dd, $J = 7.1$, 7.1 Hz, 1H; Ph), 6.99 (d, $J = 8.5$ Hz, 1H; Ph), 6.94 (dd, $J = 7.6$, 7.6 Hz, 1H; Ph), 6.91 (d, $J = 8.5$ Hz, 1H; Ph), 5.18–5.23 (m, 1H; cod-CH), 4.88–4.95 (m, 1H; 1$_A$-H), 4.44–4.50 (m, 2H; 7-H, 7′-H), 4.18–4.24 (m, 1H; 2$_A$-H), 4.01 (br s, 1H; cod-CH), 3.87 (s, 3H; OCH$_3$), 3.54 (s, 3H; OCH$_3$), 3.40–3.44 (m, 1H; cod-CH), 3.22–3.27 (m, 1H; cod-CH$_2$), 3.12–3.16 (m, 1H; cod-CH), 2.84–2.94 (m, 2H; 3$_{A,syn}$-H, cod-CH$_2$), 2.22–2.41 (m, 3H; 3$_{A,anti}$-H, 2×cod-CH$_2$), 2.04–2.12 (m, 2H; 8b-H, cod-CH$_2$), 1.85 (d, $J = 6.2$ Hz, 3H; CH$_3$), 1.60–1.68 (m, 1H; cod-CH$_2$), 1.41–1.57 (m, 2H; 2×cod-CH$_2$), 0.81 (dd, $J = 12.2$, 12.1 Hz, 1H; 8a-H), 0.43 ppm (d, $J = 7.4$ Hz, 3H; 8′-H); $^{13}C\{^1H,^{31}P\}$ NMR (125.76 MHz, [D$_8$]THF): the quaternary C atom of CF_3SO_3 could not be assigned to a ^{13}C signal; $\delta = 157.88$, 157.81, 149.86, 148.71, 133.95, 133.44, 132.96, 132.88 (s; 8×Ph), 132.83, 132.11 (d; 2× BINOL), 131.91, 130.09 (s; 2×Ph), 129.89, 129.82 (d; 2×Ph), 129.53, 129.45 (d; 2×BINOL), 128.66 (d; Ph), 127.91, 127.74, 127.69, 127.64, 126.77, 126.77 (d; 6×BINOL), 124.94 (d; Ph), 123.70 (s; Ph), 122.87, 122.40 (d; 2×BINOL), 122.21 (s; Ph), 121.36, 121.11, 111.36, 111.12 (d; 4×Ph), 107.72 (d; C-2$_A$), 102.90, 91.71, 88.23, 83.07 (d; 4×CH-cod), 76.68 (d; C-1$_A$), 60.57 (d; C-7 or C-7′), 55.61, 55.15 (q; 2×OCH$_3$), 53.10 (d; C-7 or C-7′), 44.64 (t; C-3$_A$), 37.24, 35.61, 28.47, 26.14 (t; 4×CH$_2$-cod), 19.22 (q; C-8′), 15.26 (q; CH$_3$), 12.10 ppm (t; C-8); ^{31}P NMR (202.46 MHz, [D$_8$]THF): $\delta = 123.19$ ppm; HRMS (ESI+): m/z calcd for $C_{50}H_{52}IrNO_4P^+$: 954.3258; found: 954.3294 $[M]^+$.

K4f: According to GP1 [{Ir(cod)Cl}$_2$] (33.6 mg, 50.0 μmol) and (*S*,*S*,a*S*)-**L1** (54.0 mg, 100.0 μmol) were stirred in dry THF (2.5 mL) at room temperature for 30 min. Crotyl methyl carbonate (26.0 mg, 200.0 μmol) and AgOTf (25.7 mg, 100.0 μmol) were added. After 20 h the formed white precipitate was removed by filtration, and the crude product was subjected to flash column chromatography (silica gel, dichloromethane, then dichloromethane/isopropanol 97:3) to yield **K4f** (91.2 mg, 88%) as a yellow powder containing 2% of an isomeric by-product. All analytical data given refers to a 98:2 mixture of the isomers (ratio determined by ^{31}P NMR spectroscopy). A saturated solution of **K4f** in THF, treated with benzene, deposited crystals suitable for X-ray diffraction. These were isolated by filtration. ^1H NMR (500.13 MHz, [D$_8$]THF, major isomer): $\delta = 8.36$ (d, $J = 8.8$ Hz, 1H; BINOL), 8.28 (d, $J = 8.8$ Hz, 1H; BINOL), 8.09 (d, $J = 7.7$ Hz, 1H; BINOL), 8.07 (d, $J = 7.1$ Hz, 1H; BINOL), 8.02 (d, $J = 8.8$ Hz, 1H; BINOL), 7.97 (d, $J = 8.8$ Hz, 1H; BINOL), 7.50–7.54 (m, 3H; Ph, 2×BINOL), 7.13–7.39 (m, 13H; 9×Ph, 4×BINOL), 5.13–5.17 (m, 1H; cod-CH), 4.79–4.86 (m, 1H; 1$_A$-H), 4.53 (ddd, $J = 11.5$, 11.5, 7.7 Hz, 1H; 2$_A$-H), 4.13–4.19 (m, 1H; cod-CH), 3.99 (dd, $J = 11.5$, 5.8 Hz, 1H; 7-H), 3.86–3.92 (m, 1H; 7′-H), 3.40 (dt, $J = 8.2$, 7.5 Hz, 1H; cod-CH), 3.25 (dd, $J = 14.5$, 8.5 Hz, 1H; cod-CH$_2$), 3.15 (dd, $J = 7.8$, 5.9 Hz, 1H; cod-CH), 2.86–2.94 (m, 2H; 3$_{A,syn}$-H, cod-CH$_2$), 2.32–2.41 (m, 3H; 3$_{A,anti}$-H, 2×cod-CH$_2$), 2.05 (dd, $J = 14.8$, 8.0 Hz, 1H; cod-CH$_2$), 1.92 (dd, $J = 12.3$, 5.5 Hz, 1H; 8b-H), 1.84 (br s, 3H; CH$_3$), 1.49–1.70 (m, 3H; 3×cod-CH$_2$), 1.04–1.09 (m, 1H; 8a-H), 0.57 ppm (d, $J =$ 7.4 Hz, 3H; 8′-H); $^{13}C\{^1H,^{31}P\}$ NMR (125.76 MHz, [D$_8$]THF, major isomer): $\delta = 149.89$, 148.76, 144.07, 141.41, 133.88, 133.48, 132.98 (s, 7× Ph), 132.92 (d; BINOL), 132.83 (s; Ph), 132.33 (d; BINOL), 129.56, 129.40, 129.07, 128.60, 128.14, 127.84, 127.76, 127.71, 127.67, 127.51, 126.77 (d; 5×Ph, 6×BINOL), 123.44 (s; Ph), 123.04, 122.37 (d; 2× BINOL), 122.29 (s; Ph), 107.64 (d; C-2$_A$), 103.66, 92.43, 87.87, 82.98 (d; 4×CH-cod), 77.03 (d; C-1$_A$), 66.38 (d; C-7), 60.77 (d; C-7′), 45.20 (t; C-3$_A$), 37.11, 35.34, 28.60, 26.19 (t; 4×CH$_2$-cod), 19.03 (q; C-8′), 15.14 (t; C-8), 14.95 ppm (q; CH$_3$); ^{31}P NMR (121.50 MHz, [D$_8$]THF, major isomer): $\delta = 122.80$ ppm; HRMS (ESI+): m/z calcd for $C_{48}H_{48}IrNO_2P^+$: 894.3046; found: 894.3071 $[M]^+$.

K4h: According to GP1 [{Ir(cod)Cl}$_2$] (33.6 mg, 50.0 μmol) and (*S*,*S*,a*S*)-**L2** (60.0 mg, 100.0 μmol) were stirred in dry THF (2.5 mL) at room temperature for 30 min. Cinnamyl methyl carbonate (38.0 mg, 200.0 μmol) and AgOTf (26.0 mg, 100.0 μmol) were added. After 20 h the formed white precipitate was removed by filtration, and the crude product was subjected to flash column chromatography (silica gel, dichloromethane/isopropanol 97:3) to yield **K4h** (105.0 mg, 89%) as a light yellow powder. ^1H NMR (500.13 MHz, [D$_8$]THF): $\delta = 8.39$ (d, $J = 9.2$ Hz, 1H; BINOL), 8.31 (d, $J = 9.2$ Hz, 1H; BINOL), 8.12 (d, $J = 8.1$ Hz, 1H; BINOL), 8.10 (d, $J = 8.1$ Hz, 1H; BINOL), 8.02 (d, $J = 8.9$ Hz, 1H; BINOL), 7.88–7.94 (m, 3H; BINOL, 2×Ph$_{Allyl}$), 7.24–7.58 (m, 13H; 4×Ph, 6×BINOL, 3× Ph$_{Allyl}$), 7.08–7.13 (m, 2H; 2×Ph), 6.99 (dd, $J = 7.6$ Hz, $J = 7.6$ Hz, 1H; Ph), 6.94 (d, $J = 8.4$ Hz, 1H; Ph), 5.98 (dd, $J_{P,H} = 12.1$ Hz, $J = 12.1$ Hz, 1H; 1$_A$-H), 5.33–5.41 (m, 1H; cod-CH), 4.98 (ddd, $J = 11.7$ Hz, $J = 11.6$ Hz, $J = 7.8$ Hz, 1H; 2$_A$-H), 4.69 (dd, $J = 11.7$ Hz, $J = 4.8$ Hz, 1H; 7-H), 4.53 (dq, $J_{P,H} = 21.8$ Hz, $J = 7.3$ Hz, 1H; 7′-H), 4.11 (s, 3H; OCH$_3$), 3.95–4.06 (m, 2H; 2 cod-CH), 3.58 (s, 3H; OCH$_3$), 2.74–2.91 (m, 4H; 3$_{A,syn}$-H, cod-CH, cod-CH$_2$), 2.56–2.67 (m, 1H; cod-CH$_2$), 2.43 (d, $J = 10.9$ Hz, 1H; 3$_{A,anti}$-H), 2.05–2.35 (m, 3H; 8b-H, 2 cod-CH$_2$), 1.36–1.79 (m, 3H; 3 cod-CH$_2$), 0.91 (dd, $J = 12.4$ Hz, $J = 11.7$ Hz, 1H; 8a-H), 0.49 ppm (d, $J =$ 7.5 Hz, 3H; 8′-H); ^{13}C $\{^1H, ^{31}P\}$ NMR (125.76 MHz, [D$_8$]THF): $\delta =$ 157.85, 157.77, 149.84, 148.69 (4s; Ph), 136.00 (s; Ph$_{Allyl}$), 133.97, 133.42, 133.08, 133.04 (4s; Ph), 132.92, 132.14 (d; 2×BINOL), 131.76 (s; Ph), 130.09, 130.01, 129.91, 129.91, 129.69, 129.59, 129.45, 129.24, 128.77 (8d; 3×Ph, 2×BINOL, 3×Ph$_{Allyl}$, s; Ph), 127.98, 127.76, 127.71, 127.69, 126.85, 126.81 (d; 6×BINOL), 124.86 (d; Ph), 123.75 (s; Ph), 123.01, 122.28 (2d; BINOL), 122.14 (s; Ph), 121.49, 121.30, 111.26, 111.21 (d; 4×Ph), 102.43 (d; CH-cod), 98.26 (d; C-2$_A$), 92.72, 90.39 (d; 2×CH-cod), 86.52 (d; C-1$_A$), 83.60 (d; CH-cod), 60.48 (d; C-7), 55.74, 55.21 (q; 2×OCH$_3$), 53.22 (d; C-7′), 41.16 (t; C-3$_A$), 35.60, 34.01, 28.41, 26.85 (t; 4×CH$_2$-cod), 19.22 (q; C-8′), 14.78 ppm (t; C-8); ^{31}P NMR (121.50 MHz, [D$_8$]THF): $\delta =$ 120.15 ppm; HRMS (ESI+): m/z calcd for $C_{48}H_{48}IrNO_2P^+$: 1016.3414; found: 1016.3420 $[M]^+$.

Acknowledgements

This work was supported by the Fonds der Chemischen Industrie, the Deutsche Forschungsgemeinschaft (SFB 623), the Studienstiftung des Deutschen Volkes (J.A.R.) and the Landesgraduiertenförderung (S.S.). We thank Prof. B. F. Straub and Dr. M. Hofmann for helpful discussions.

[1] Reviews: a) G. Helmchen, A. Dahnz, P. Dübon, M. Schelwies, R. Weihofen, *Chem. Commun.* **2007**, 675; b) G. Helmchen in *Iridium Complexes in Organic Synthesis* (Eds.: L. A. Oro, C. Claver), Wiley-VCH, Weinheim, **2009**, pp. 211–250; c) R. Takeuchi, S. Kezuka, *Synthesis* **2006**, 3349; d) H. Miyabe, Y. Takemoto, *Synlett* **2005**, 1641.

[2] C. Welter, O. Koch, G. Lipowsky, G. Helmchen, *Chem. Commun.* **2004**, 896.

[3] C. A. Kiener, C. Shu, C. Incarvito, J. F. Hartwig, *J. Am. Chem. Soc.* **2003**, *125*, 14272.

[4] S. Spiess, C. Welter, G. Franck, J.-P. Taquet, G. Helmchen, *Angew. Chem.* **2008**, *120*, 7764; *Angew. Chem. Int. Ed.* **2008**, *47*, 7652.

[5] R. Weihofen, O. Tverskoy, G. Helmchen, *Angew. Chem.* **2006**, *118*, 5673; *Angew. Chem. Int. Ed.* **2006**, *45*, 5546.

[6] J. Tsuji, I. Minami, I. Shimizu, *Tetrahedron Lett.* **1984**, *25*, 5157.

[7] DFT calculations have been carried out on chiral intermediates of Ir-catalysed allylic substitutions that have not been substantiated experimentally: a) N. Kinoshita, K. H. Marx, K. Tanaka, K. Tsubaki, T. Kawabata, N. Yoshikai, E. Nakamura, K. Fuji, *J. Org. Chem.* **2004**, *69*, 7960; b) M. Kimura, Y. Uozumi, *J. Org. Chem.* **2007**, *72*, 707.

[8] S. Spiess, J. A. Raskatov, C. Gnamm, K. Brödner, G. Helmchen, *Chem. Eur. J.* **2009**, *15*, 11087.

[9] a) D. Polet, A. Alexakis, K. Tissot-Croset, C. Corminboeuf, K. Ditrich, *Chem. Eur. J.* **2006**, *12*, 3596; b) K. Tissot-Croset, D. Polet, A. Alexakis, *Angew. Chem.* **2004**, *116*, 2480; *Angew. Chem. Int. Ed.* **2004**, *43*, 2426.

[10] D. Marković, J. F. Hartwig, *J. Am. Chem. Soc.* **2007**, *129*, 11680.

[11] S. T. Madrahimov, D. Marković, J. F. Hartwig, *J. Am. Chem. Soc.* **2009**, *131*, 7228.

[12] The complex **K1H** does not seem to affect further transformations. In the following the mixture of **K1** and **K1H** as depicted in Figure 1 A is designated **K1**.

[13] **K5** is, of course, the first product of the substitution reaction. The fact that it was not found in the reaction mixture to a significant extent during the reaction suggested the possibility that it is formed by a reaction between **K1** or **K2** and the decomplexed reaction product **2**. To test this possibility, **K1** was generated by mixing [{Ir(cod)Cl}$_2$] and **L2** (2 equiv) in THF; then an excess of the branched amination product **2**, Nu = HNBn or HNPh, and TBD (3–4 equiv), were added. Indeed, **K5** was found to be the main species of the mixture after 1–2 h (^{31}P NMR spectroscopy; see the Supporting Information). For further experiments concerning this issue see the Supporting Information of reference [10].

[14] Treatment of a complex **K1** containing the ligand (*aR*,*S*,*S*)-**L1** with $AgSbF_6$ in CH_2Cl_2 does not effect C–H activation; a complex [Ir(cod)(*aR*,*S*,*S*)-**L1**]SbF_6 is formed (see, Scheme 3, lower left), which is stabilised by a Ph→Ir coordination. See: T. Osswald, H. Rüegger, A. Mezzetti, *Chem. Eur. J.* **2010**, *16*, 1388.

[15] We have earlier prepared and structurally characterised a (π-allyl)Ir complex with a PHOX ligand. Dimethyl malonate reacted with this complex at the central rather than the terminal allylic carbon, see C. Garcia-Yebra, J. P. Janssen, F. Rominger, G. Helmchen, *Organometallics* **2004**, *23*, 5459; for a (π-allyl)Ir complex containing a pybox ligand see P. Paredes, J. Díez, M. P. Gamusa, *Organometallics* **2008**, *27*, 2597.

[16] Remarkably, crystals were only obtained if benzene was contained in the solvent, see reference [11].

[17] T. Ohmura, J. F. Hartwig, *J. Am. Chem. Soc.* **2002**, *124*, 15164.

[18] To test for identity of the crystal structure and the structure in solution, a crystal of complex **K4a** was dissolved in [D_8]THF in an NMR tube at −80 °C, and the solution was allowed to warm up to RT. Excepting line broadening due to the low temperature, ^{31}P NMR spectra did not change.

[19] a) B. Bartels, C. Garcia-Yebra, G. Helmchen, *Eur. J. Org. Chem.* **2003**, 1097; b) A. Leitner, C. Shu, J. F. Hartwig, *Proc. Natl. Acad. Sci. USA* **2004**, *101*, 5830.

[20] M. J. Pouy, L. M. Stanley, J. F. Hartwig, *J. Am. Chem. Soc.* **2009**, *131*, 11312.

[21] The first two allylic complexes were obtained through replacement of the PMe_3 ligand by an unsubstituted allylic moiety, yielding the Δ-P-*endo* and Δ-P-*exo* diastereomers. Geometric alterations within these two complexes were conducted by 1) altering the helicity (Λ or Δ) of the complex through the appropriate modifications of the coordination for both cod and the allylic fragment and 2) rotating the Ir(*C*,*P*-**L1**) fragment so that one of the allylic termini occupied the coordination site *trans* to the CH_2 group of the chiral ligand. The conformation of the chiral ligand backbone and the five-membered iridacycle were kept within the crystallographically determined conformation.

[22] a) J. B. Wakefield, J. M. Stryker, *J. Am. Chem. Soc.* **1991**, *113*, 7057; b) E. B. Tjaden, K. E. Schwiebert, J. M. Stryker, *J. Am. Chem. Soc.* **1992**, *114*, 1100; c) E. B. Tjaden, J. M. Stryker, *J. Am. Chem. Soc.* **1990**, *112*, 6420.

[23] A. D. Becke, *J. Chem. Phys.* **1993**, *98*, 1372; A. D. Becke, *J. Chem. Phys.* **1993**, *98*, 5648.

[24] C. Lee, W. Yang, R. G. Parr, *Phys. Rev. B* **1988**, *37*, 785.

[25] Gaussian 03, Revision B.03, M. J. Frisch, G. W. Trucks, H. B. Schlegel, G. E. Scuseria, M. A. Robb, J. R. Cheeseman, J. A. Montgomery, Jr., T. Vreven, N. Kudin, J. C. Burant, J. M. Millam, S. S. Iyengar, J. Tomasi, V. Barone, B Mennucci, M. Cossi, G. Scalmani, N. Rega, G. A. Petersson, H. Nakatsuji, M. Hada, M. Ehara, K. Toyota, R. Fukuda, J. Hasegawa, M. Ishida, T. Nakajima, Y. Honda, O. Kitao, H. Nakai, M. Klene, X. Li, J. E. Knox, H. P. Hratchian, J. B. Cross, V. Bakken, C. Adamo, J. Jaramillo, R. Gomperts, R. E. Stratmann, O. Yazyev, A. J. Austin, R. Cammi, C. Pomelli, J. W. Ochterski, P. Y. Ayala, K. Morokuma, G. A. Voth, P. Salvador, J. J. Dannenberg, V. G. Zakrzewski, S. Dapprich, A. D. Daniels, M. C. Strain, O. Farkas, D. K. Malick, A. D. Rabuck, K. Raghavachari, J. B. Foresman, J. V. Ortiz, Q. Cui, A. G. Baboul, S. Clifford, J. Cioslowski, B. B. Stefanov, G. Liu, A. Liashenko, P. Piskorz, I. Komaromi, R. L. Martin, D. J. Fox, T. Keith, M. A. Al-Laham, C. Y. Peng, A. Nanayakkara, M. Challacombe, P. M. W. Gill, B. Johnson, W. Chen, M. W. Wong, C. Gonzalez, J. A. Pople, Gaussian, Inc., Wallingford CT, **2004**.

[26] a) R. Ditchfield, W. J. Hehre, J. A. Pople, *J. Chem. Phys.* **1971**, *54*, 724; b) W. J. Hehre, R. Ditchfield, J. A. Pople, *J. Chem. Phys.* **1972**, *56*, 2257; c) P. C. Hariharan, J. A. Pople, *Theo Chim. Acta* **1973**, *28*, 213; d) P. C. Hariharan, J. A. Pople, *Mol. Phys.* **1974**, *27*, 209; e) M. S. Gordon, *Chem. Phys. Lett.* **1980**, *76*, 163.

[27] D. Andrae, U. Haeussermann, M. Dolg, H. Stoll, H. Preuss, *Theor. Chim. Acta* **1990**, *77*, 123.

[28] C. Y. Peng, H. B. Schlegel, *Isr. J. Chem.* **1994**, *34*, 449.

[29] C. Benzi, M. Cossi, V. Barone, R. Tarroni, C. Zannoni, *J. Phys. Chem. B* **2005**, *109*, 2584.

[30] J. Tomasi, B. Mennucci, R. Cammi, *Chem. Rev.* **2005**, *105*, 2999.

[31] H. E. Gottlieb, V. Kotylar, A. Nudelman, *J. Org. Chem.* **1997**, *62*, 7512.

[32] S. Berger, *Angew. Chem.* **2004**, *116*, 2070.

[33] SADABS 2008/1, G. M. Sheldrick, Bruker Analytical X-ray Division, Madison, Wisconsin **2008**.

[34] SHELXTL 2008/4, G. M. Sheldrick, *Acta Crystallogr. Sect. A* **2008**, *64*, 112.

[35] C. Gnamm, G. Franck, N. Miller, T. Stork, K. Brödner, G. Helmchen, *Synthesis* **2008**, 3331.

[36] C. Gnamm, S. Förster, N. Miller, K. Brödner, G. Helmchen, *Synlett* **2007**, 790.

Received: December 17, 2009
Published online: April 23, 2010

